Master Thesis in Geosciences

Structure and Microseismicity of the unstable rock slide at Åknes, Norway

Marianne Holst Nielsen

UNIVERSITY OF OSLO

FACULTY OF MATHEMATICS AND NATURAL SCIENCES

Structure and Microseismicity of the Unstable Rock slide at Åknes, Norway

Marianne Holst Nielsen

Master Thesis in Geosciences

Discipline: Petroleum Geology and Geophysics

Department of Geosciences

Faculty of Mathematics and Natural Sciences

UNIVERSITY OF OSLO

15th of December 2008

Abstract

The Åknes site is a potential rockslide in a hillside of a fjord on the west coast of Norway in the county of Møre Og Romsdal. A rockslide at Åknes has the potential of making a large flood wave. The flood wave could destroy the closest villages and kill many people. Due to this big threat the area has been heavily investigated by numerous methods since it was discovered in 1985 by NGI. Among these investigations a passive seismic network for monitoring the microseismicity of the area was temporarily installed in 2005, recording seismic data for 6-7 weeks. The dataset from this acquisition has been analyzed in this thesis. 7 microseismic events have been detected with an algorithm which uses the STA/LTA method. From the information on five shots of a refraction seismic survey executed the last two days of the passive networks recording period, has been used to make a traveltime-distance plot for the whole area. From this plot a velocity model has been made. By using the relation between traveltime and epicentral distance, found from the five shots, the detected events have been localized by using a misfit function.

Sammendrag

På Åknes i Møre og Romsdal, Norge, er det i dalsiden av en fjord oppdaget et potensielt fjellskred. Et ras på Åknes kan lage en enorm flodbølge nede i fjorden. Denne flodbølgen vil ødelegge de nærmeste bygdene og mange menneskeliv vil gå tapt. Området ble i 1985 først undersøkt av NGI. På grunn av den potensielle faren fra Åknes, så har området siden den gang blitt grundig undersøkt med mange ulike metoder. Blant disse undersøkelsene ble det i 2005 utplassert midlertidig et passivt seismisk nettverk for å undersøke områdets mikroseismisitet. Nettverket registrerte seismisiteten i 6-7 uker. Datasettet fra denne undersøkelsen er blitt analysert i denne oppgaven. Det er blitt funnet 7 mikroseismiske hendelser i dataene ved å bruke en algoritme som benytter seg av STA/LTA metoden. I løpet av de to siste dagene av registreringstiden til det passive nettverket ble det utført refraksjonsseismikk med fem aktive skudd. Informasjon om disse skuddene er brukt til å lage et gangtid-avstandsplott som omfatter hele området. Fra dette plottet er det laget en hastighetsmodell. Ved å bruke forholdet mellom gangtid og episentrisk avstand, som ble funnet i gangtid-avstansplottet, så har man ved hjelp av en mistilpassningsfunksjon lokalisert de seismiske hendelsene.

CONTENT:

1: INTRODUCTION

1.1: Rock slides in western Norway

The west coast of Norway is the land of the fjords. The fjords on the west coast of Norway were created during periods with ice coverage in the Quaternary (from two million years ago). Arms from the bigger inland ice have dug deep valleys into the bedrock, and the glacier tongue has been in direct contact with the sea. Sediments transported by the ice created an end moraine under the glacier tongue creating a shallow area as the ice melted and the sea flooded the valley. The valleys are deep U-valleys with steep slopes at the sides filled with deep calm blue/green tainted sea water. Because of the steep slopes and depending on the properties of the soils and the bedrock in the area, many of these valleys have unstable rock masses in the hillsides. This results in a constant occurrence of rock falls and slides of different sizes and nature. Rock slides in some remote places would maybe do no significant damage, but rock slides of the same size plunging into the fjords have the potential of making large flood waves, which in turn are a threat to villages in the fjord valleys and users of the fjords. If you drop a mass of stone into open waters, the energy of the resulting wave will spread out in a 3D hemisphere, but if you drop the same mass into a fjord, the energy from the resulting wave will spread out in a 2D-like tube and the wave will have a height many times as high than in open waters. Bathymetric measurement of the bottom of the fjords shows a history of rock slides (Delarue, 2006). During the last century, rock slides and the following flood waves in the fjords have killed 175 people (Delarue, 2006). In 1934 a rock fall at Langhammaren in the Tafjord, Western Norway, killed 50 people and made enormous damages to three villages (Furseth, 1985). The size of the rock masses of the 1934 slide was estimated to be about 3 million m^3 and the flood wave had a maximum height of more than 60 m (Furseth, 1985).

1.2: Åknes

In the same area as the Tafjord, we have today a large potential rock slide at the Åknes site. Among the areas that will suffer by a slide at Åknes is the Geiranger fjord which is one of Norway's largest tourist attractions. In high season the cruise ships practically wait in line to sail in the fjord with thousands of tourists. Some of the ships even make a comment to the

tourists, while they sail past the Åknes site, of the danger hanging in the hillside. The Geiranger Fjord was in 2005 put on UNESCO's World Heritage List. Due to the threat to people and nearby villages the Åknes site has been investigated by a number of methods since 1985, when the first geological mapping was carried out by NGI. The Åknes rockslide has become one of the most investigated in the world, making it a naturally laboratory for researches from all over the world. In the present study I will analyze microseismic data from a temporary seismic network installed in 2005. This was installed just before another permanent seismic network was installed, one which is operative today and which has been studied by Michael Roth (NORSAR, Kjeller & ICG, Oslo, Norway). To get an overview of the area to be studied I will introduce some details of the morphology and geology at the Åknes site. Åknes is located in the same fjord system as the Tafjord, the Inner Storfjord System on the west coast of Norway in the county of Møre og Romsdal. Figure 1.1 shows the location.

Figure 1.1: The location of the Åknes site (Roth etal., 2006).

The flood wave created by a possible rockslide at Åknes would make a lot of material damage and put many lives at risk. The size of the instable masses has been estimated to have a volume of 35-40 million m^3 (Darron etal., 2005). This is the estimation used in the latest article (Ganerød etal., 2008), but there have been several estimations, some up to 100 million m^3. If this block should fall into the fjord in one piece, which is the worst case scenario, a flood wave with a maximum height of 90m could be created (Eidsvig & Harbitz, 2005). If you compare this to the volume of the Tafjord slide in 1934 you get an idea of the possible damage a slide at Åknes would cause.

The instable area at Åknes is about 1 km^2 and the slope is dipping towards south with an average slope of 30-35˚ (Ganerød etal., 2008). Figure 1.2 shows a picture of the area taken

from SE. The upper boundary of the area is about 800 m long and 500 m of it is defined by a big open fracture, which shows both horizontal and vertical separation. The fracture width increases from east to west, from 0.5-1 m in the east to 20-30 m in the west (Ganerød etal., 2008). The western boundary is defined by a strike slip fault which is striking NNW-SSE. This fault is old, probably from Devonian age, and it exceeds the extension of the area as it can be traced as a lineament for several km (Ganerød etal., 2008). The fault can be seen in the picture in figure 1.2 as a crevasse on the left side of the area, marked by a red line. The eastern boundary is also defined by a fault. This is a gently dipping NNE-SSW trending fault which can be seen as a zone with heavily fractured rocks (Ganerød etal., 2008). The lower boundary is defined where a major sliding surface reaches the surface. It can bee seen at places where rocks above the sliding surface are being pushed outwards and down the slope creating overhangs (Ganerød etal., 2008).

Figure 1.2: Picture of the slope taken from the south. Upper right corner
shows a close-up of the open fracture limiting the area to the north (Roth, 2005).

The geology in the area is that of old gneisses. The gneisses are metamorphosed rocks, of magmatic origin, that formed the base of the Caledonian mountain chain when it was created about 400 million years ago (Tveten etal., 1998). Figure 1.3 shows a geological map over the area around the Åknes site. During the Caledonian orogeny, the gneisses at Åknes were

heavily foliated and folded. The gneisses vary from medium grained granitic gneiss to hornblende/biotite bearing medium grained dioritic gneiss, and you can also find up to 20 cm thick layers of biotite schist (Ganerud etal., 2008). At Åknes the foliation is subparallel to the surface and all the lithologies are in layers parallel to the foliation. The sliding surface has developed as a consequence of this geological setting together with the faults described above, with sliding starting in the weakest layers of the foliation. The total block which is moving can be divided into two smaller blocks with different rates of movement, one in the NW corner with a moving rate of 7-20 cm/year, and one bigger one comprising the main part of the area that moves 1-4 cm/year (Blikra, 2006). Figure 1.4 shows the two blocks with different colours.
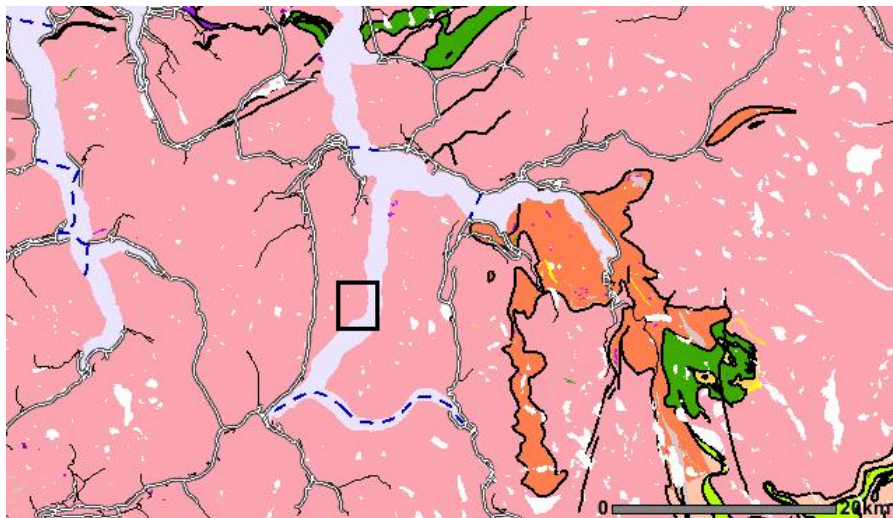
Figure 1.3: A geological map around the Åknes site, marked with a black square.
The pink in the map is diorittic to granittic gneiss and migmatits. The orange area
are eyegneiss, granite and folieted granite. The green area are amfibolite and glimmer
slate (NGU, 2008).
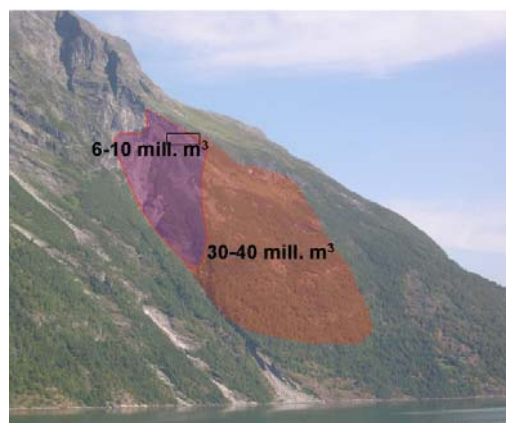
Figure 1.4: The instable are is divided into two smaller blocks,
the smallest one in purple and the bigger one in orange (Blikra, 2006).

1.3: Gathering of passive seismic data

In 2005 a permanent seismic network for monitoring the microseismic activity of the slope was installed. Microearthquakes are defined as a local earthquake with a magnitude of less than 2.5. This network consists of eight 3-component geophones installed in the upper part of the area, covering about 250 m x 150 m (Roth elat., 2005). When the unstable masses at Åknes move, they move in tiny steps which creats microseismic earthquakes. By measuring the rate of microseismic activity, one can say something about the rate of movement in the slide (Roth, 2006). This network is now incorporated in a warning system, so that if the seismic activity suddenly should increase and one expects the slide to accelerate, the people living in the villages in the area can get a chance to evacuate.

Another seismic network, covering a larger area, was installed temporarily in 2005. This was done in a project called "Geophysics for investigation and analysis of large landslides" which was started in 2005 by the researchers at NORSAR and ICG (International Centre of Geohazard), in coorporation with french colleagues at LGIT (Laboratoire de Géophysique Interne et Tectonophysique, Grenoble). The aim of the project was to share mutual experience in the use of geophysics in landslides (Lecomte, 2006), and Åknes was a natural laboratory for this project. The aim of the project was especially to work on background seismic noise, microseismic monitoring and seismic tomography, to better model the rupture surface and internal deformations and to better understand the movement pattern of the unstable block (Lecomte, 2006). During a mission to the Åknes site, 19/8-05 to 6/9-05, an IHR (Réseau d'Imagerie de Haute Résolution) network provided by LGIT was installed. The network acquired passive seismic data continuously for 6-7 weeks and was also used for a short refraction seismic experiment 15th to 18th of October 2005. After October the site is inaccessible because of snow. All the data from the IHR network had for different reasons not yet been processed and analyzed, except for the recordings of the refraction seismic (Frery, 2007). The first analysis of the passive seismic, i.e., the recording of the micro seismic activity during these 6-7 weeks has been done during the work of this thesis.

The IHR network consisted of ten stations, each is having nine channels associated with six one-component vertical geophones and one three-component geophone. Actually the whole IHR system consists of 30 stations but the Åknes site is a difficult area to work in so managing to deploy as much as 10 stations demanded a great effort. Figure 1.5 shows the

different elements of each station. The IHR stations have a new acquisition system made for difficult hazardous sites, and have a large number of available recording channels and wireless communication between the stations (Brenguier etal, 2005). The stations were spread out as evenly as possible over the area as shown in Figure 1.6. The stations are mostly organized with the three-component geophone in the centre and the vertical component geophones in a star like pattern around it (every 60˚) with cables of 30 to 50m (Roth etal, 2006) The geophones are marked with red and green crosses in figure 1.5. The horizontal positions of the sensors were measured by differential GPS with an error of less than 15cm. and the elevation was taken from a high resolution digital elevation map made by an airborne laser scanner in 2004 (Frery, 2007). The geophones where all shielded with plastic containers to keep the temperature and to minimize noise from wind.
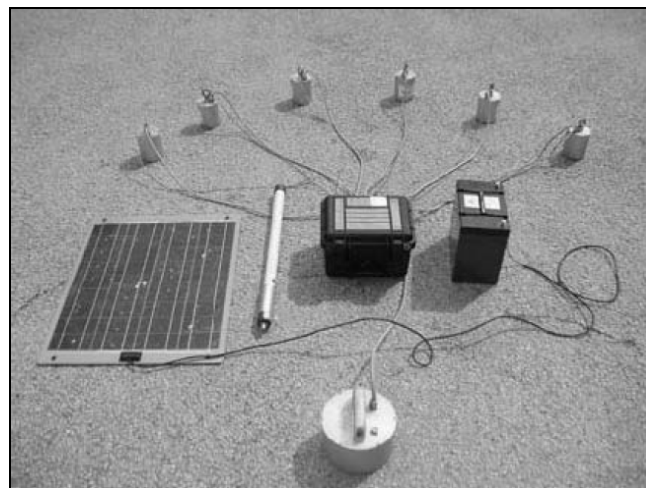
Figure 1.5: The elements of one station in the IHR network.
The stations were powered by a solar panel.
The white rod is the radio antenna (Roth etal., 2006).

From a temporarily seismic pilot installation in 2004 it was clearly seen that the frequencies of the microseismic events are well above 10Hz (Delarue, 2006). So a high sampling rate was needed, which the IHR system can provide, and the stations were set to record with a sampling interval of 4 ms (Frery, 2007).
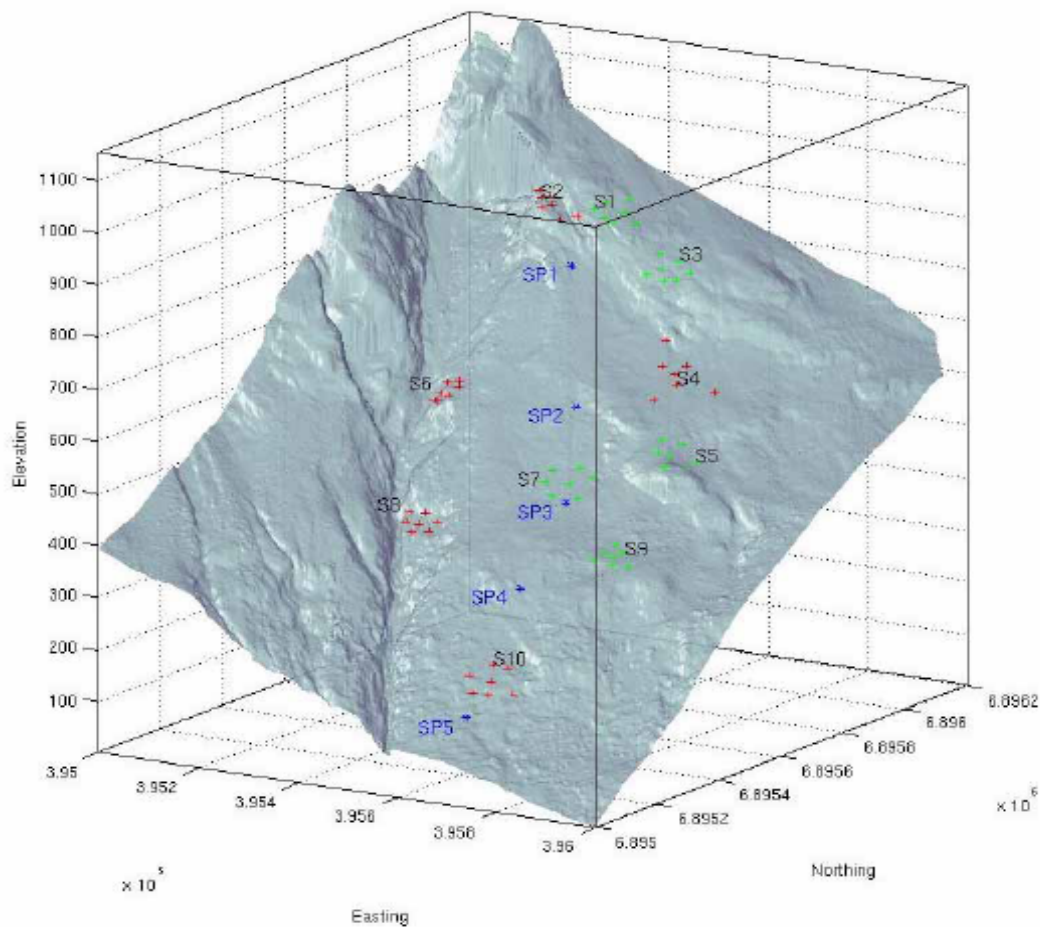
Figure 1.6: The deployment of the stations S1 to S10 with the geophones marked with red and green crosses. The shots from the refraction seismic survey SP1 to SP5 in blue (Frery, 2007)

During the last mission, just before the IHR network was dismantled, a seismic refraction survey was put up. This was done along a 470 m long line in the centre of the area, from an altitude of 300m to 580m above see level (Roth etal., 2005). In figure 1.6 the shots are marked in blue with SP1 to SP5. Figure 1.7 shows the seismic section from SP1. There is a clear brake in the first arrivals for trace nr 12 at 0.1s, where the slowness of first arrival times starts to increase. Otherwise the first arrival times change quite regularly with increasing offset. This indicates a velocity model with at least two layers of different velocities, a layer with low velocity on top over a layer with higher velocity (Roth, 2006). An interpretation on the velocities from this survey will be used for comparison to the velocity model made I chapter 3
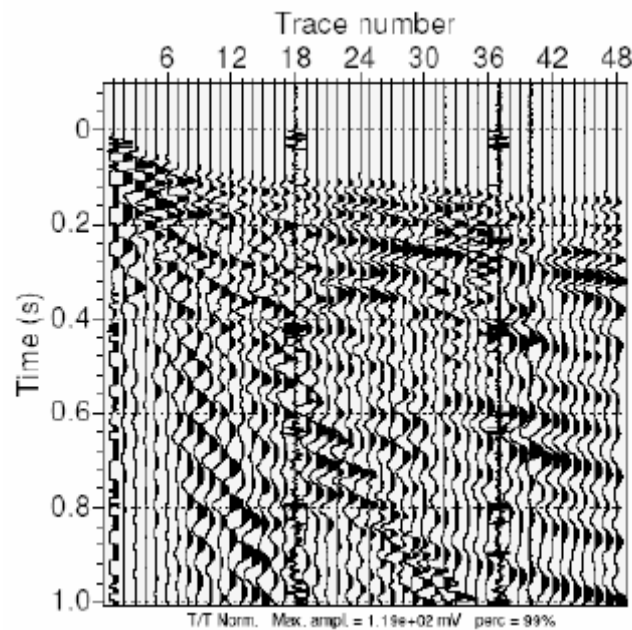
Figure 1.7: Seismic section of SP2 showing a break in the arrival times for receiver 12 at 0,1sec (Dietrich et al. 2005)

1.4: Objectives

During the work of this thesis the passive seismic data gathered by the IHR network in 2005 were analyzed. The goal was to find microseismic events in the data that are associated with the movement of the rock slide at Åknes. To do this a method for automatically finding the events in the data needed to be developed. Microseismic events had then to be localized. If events are found and successfully localized, something can be said about the nature of the movement of the slide. By locating an event one can say where the slide is active. The final goal is to use the rate of microseismic events to reveal where the movement rate is highest. If the hypocentre (the depth and position of an earthquake) can be mapped, one could also determine the detachment zone. Seismic data alone may not be enough to accurately determine the detachment zone but together with resistivity measurement, GPR measurement, seismic refraction and tomography, and borehole analysis, the result can be quite robust.

2: DETECTING EVENTS

2.1: Method for detecting events

The dataset was converted from its original form to SAC (Seismic Analysis Code) format by Olivier Coutant at LGIT (Laboratoire de Géophysique Interne et Tectonophysique), Grenoble, in May 2008. Each sac-file contains data for one hour (900000 sampling points) from one component. Each station has one directory, each of these contains one directory for each day, and each day-directory contains the sac-files for every hour. The title of each file contains information about the data and time, the station nr and the component nr.

The full amount of data was approximately a half of a terra byte. That is a lot of data and given the limited amount of time for the present work, it was not possible to analyse all of the data. So it was necessary to make a reasonable selection on what data to analyse and what to leave for later work. The first decision was to only use the data from the 11 hours during night time, from seven in the evening to seven in the morning. The reason behind this decision was that during daytime there was quite a bit of field work going on making a lot of noise on the data, at the time of recording because of extensive activities at Åknes in 2005 with various investigations and well boring, in addition to helicopter transport. This gives 250 Gbytes to work with.

2.1.1: The STA/LTA method

STA/LTA is short for Short-term Average over Long-Term Average. The purpose of this method is to automatically detect when the amplitude of the seismic signal suddenly increases. The method works by going through the seismogram, calculating the average of the amplitude over two different time windows, and when the ratio between these two averages (called STA/LTA) exceeds a certain value a registration of the time is triggered. The method is useful when the target events are not exclusively the ones with the biggest amplitude, and it can also to some extent help to distinguish between different types of earthquakes (Trnkoczy, 1998). In this method there are five parameters to set:

STA-window duration in time

LTA-window duration in time

STA/LTA trigger threshold level

STA/LTA detrigger threshold level.

Relative position between the STA and the LTA windows

The first two parameters are the two time windows over which the average of the amplitudes are calculated. STA is an average over a short time window and LTA is an average over a long time window. The second two parameters are the value of ratios that trigger and detrigger the registration of an event. When the STA/LTA exceeds a certain value (the trigger threshold level), the time is registered as the beginning of an event. When the STA/LTA reaches a value below detrigger threshold level, the time is registered as the end of an event. The parameters need to be chosen carefully to fit the type of waveforms that are the target events. The STA time window needs in general to be a few periods longer than the expected dominant period of a target event (Trnkoczy, 1998). By choosing a short LTA we make the trigger more sensitive to short lasting local events with high frequency. If you were to be interested in long period low frequency earthquake signal, the LTA would need to be longer (Trnkoczy, 1998).

When the LTA is much longer than the longest duration of an event it represents the average background noise level, and will not be very sensible to sudden changes in the amplitude (Ambuter & Solomon, 1974). The STA will quickly respond to an increase in amplitude. As you move in steps across the seismogram, continuously calculating the STA and the LTA, the STA/LTA will have a value close to one when there are no events, but it will increase suddenly when an event occurs and the value of STA increases while the LTA stays close to the same.

2.1.2: Algorithm for detecting events

The algorithm was divided into four parts:

Part 1) Convert the sac-files into proper format for the chosen programming language.

Part 2) Make a program that goes through the data using the STA/LTA method and register the times of the events and the header-information in a matrix.

16

Part 3) Automatically run part 1) and 2) for several sac-files and write matrices with the registered events in a file.

Part 4) Sort out the resulting files containing the registered events.

Part 1) Matlab was the programming tool I choose to use, since this is the tool I am most familiar with. To read sac-files into matlab, an already existing program called rsac.m was used (Thorne, 2004). This program formats the sac files into a matrix with three columns. The first column holds the time values, the second one holds the amplitude values, and the third one holds the header information. A figure can be made of the seismic trace by plotting the time values vs. the amplitude values. The matrix was then used as input argument in the program findevents.m which goes through the sac file using the STA/LTA method.

Part 2) The program findevents.m was written as a function with the sacfile-matrix and the filenames of the sac-file as input arguments. The program can be found in appendix A.2.

It was important when making this program to have in mind the amount of data (250 Gb) to be processed, and to reduce computing time as much as possible on each sac-file. This means among other things keeping the for-loops and if-tests as simple and as few as possible.

First the four STA/LTA parameters were determined according to the theory above and from information of what is used on the permanent seismic network at Åknes (Roth, personal communication). The local microseismic events most suitable for localization have durations of less than two seconds (Delarue, 2006). So the parameters where set to:

STA time window = 0.25 s
LTA time window = 2 s
STA/LTA trigger threshold = 3
STA/LTA detrigger threshold = 3

The relative position in time of the short term window and the long term window had also to be chosen. There are two possible realative positions, as illustrated as line pieces in figure 2.2.1. One way is to let the STA end at the same time as the LTA ends. Another way is to let the STA begin where the LTA ends.
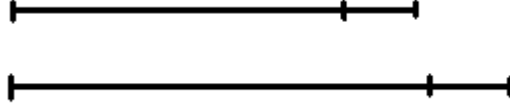
Figure 2.2.1: The five ways of calculating the STA/LTA. Five is the lowest one.

The first configuration was chosen because this seemed to be the fastest and easiest one to program. What could have been done is to test out if choosing one or the other method had any impact on the registration of an event. I suspect that if the LTA is chosen correctly it should represent the background noise and not be affected by an event, and the choice of method would only have affects on when the trigger threshold and detrigger threshold is reached.

The calculation of STA and LTA is made inside a for-loop going through the sacfile. For every 40 ms (every 10th sampling point) the STA, LTA and the STA/LTA is calculated using equations 1 and 2.

$$LTA = \sqrt{\frac{1}{n_1 - 1} \sum_{l=i}^{i+n_1} (x_l - \bar{x})^2} \qquad \text{(Equation 1)}$$

Where:

$$\bar{x} = \frac{1}{n_1} \sum_{l=i}^{i+n_1} x_l \qquad \text{(Equation 2)}$$

X_l are the sampled signal and n_1 is the length of the LTA time window in sampling points. Similarly the STA is calculated by using equations 3 and 4.

$$STA = \sqrt{\frac{1}{n_2 - 1} \sum_{l=i+n_1-n_2}^{i+n_1} (x_l - \bar{x})^2} \qquad \text{(Equation 3)}$$

Where:

$$\overline{x} = \frac{1}{n_2} \sum_{l=i+n_1-n_2}^{i+n_1} x_l$$
<div align="right">(Equation 4)</div>

Where n_2 is the length of the STA time window in sampling points. When calculating the STA and LTA using equations 1 and 3 the mean amplitude is subtracted. The reason for this is that the amplitude does not always oscillate around zero. Figure 2.2 shows an example of this.

To be able to get a correct trigger time and a correct detrigger time compared to the actual event, one might let the LTA stay constant from when trigger threshold is reached until detrigger threshold is reached. This required an extra if-test inside the for-loop going through the sacfile, and this element was dropped to save calculating time. To save even more time I tried out to calculate the LTA outside the for-loop as an average of the whole sac-file and let the value of LTA be constant when calculating the STA/LTA inside the loop. The idea was that since the LTA is supposed to represent the background noise, it should not change significantly through one sac-file, because it is only one hour long. But it turns out that the noise level changes throughout the sac file. The result was triggering when there were no event (where the background noise level decreased), and missing out events where the background noise level increased compared to the amplitude of the event.

The final chosen configuration was to run, by going through the sac-file matrix every 10th sampling point, calculating the LTA, the STA and the STA/LTA. If the STA/LTA exceeds the value 3, the time is registered in a matrix called "event" as the starting point of an event, and when STA/LTA reaches a value below 3 the time is registered in the event matrix as the ending point of the same event. Figure 2.1 to 2.3 shows three examples of how the STA/LTA varies during one hour and the corresponding seismogram. When the noise level was high and contained a lot of spikes, many "false" events were registered as in figure 2.1. On the noisiest days up to 20 "false" events were registered per hour. Figure 2.2 shows how the STA/LTA reacts when a possible microseismic event is registered on the seismogram. Figure 2.3 show that the STA/LTA also exceeds a value of 3 for local earthquakes.

/media/ICG$_A$aknes/S1/248/2005.09.05-05.59.59.S1.00.03.SAC
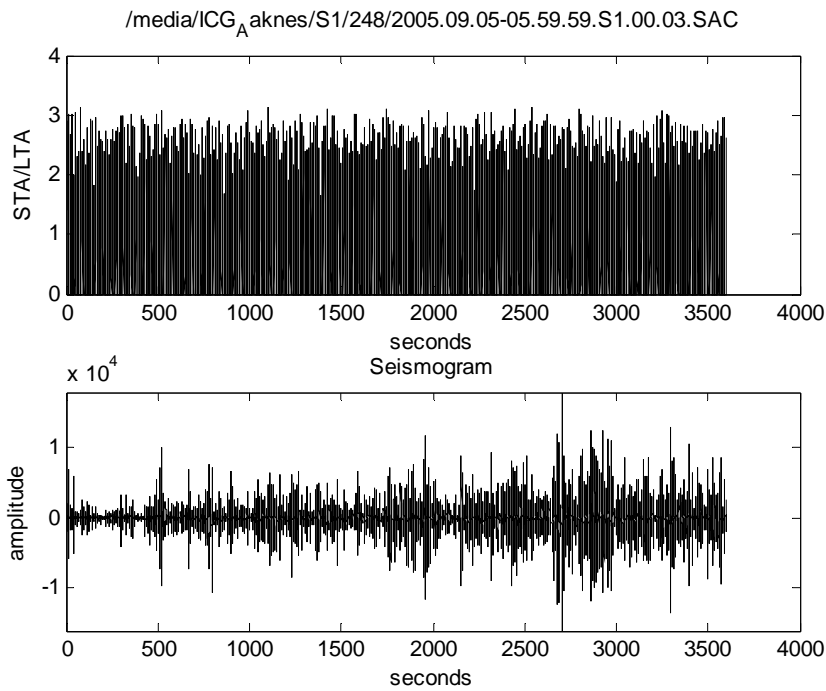
Figure 2.1: The upper part of the figure shows the value of the STA/LTA as it is calculated for all the sampling points during one hour. The lower part of the figure shows the corresponding seismogram. This is an example of very noisy data, recorded from component nr 3 at station S1, with starting time 05.59.59, day nr 248 which is 5th of September 2005. Here many "false" events have been registered as the STA/LTA has reached values over 3.

/media/ICG$_A$aknes/S1/248/2005.09.05-02.59.59.S1.00.05.SAC
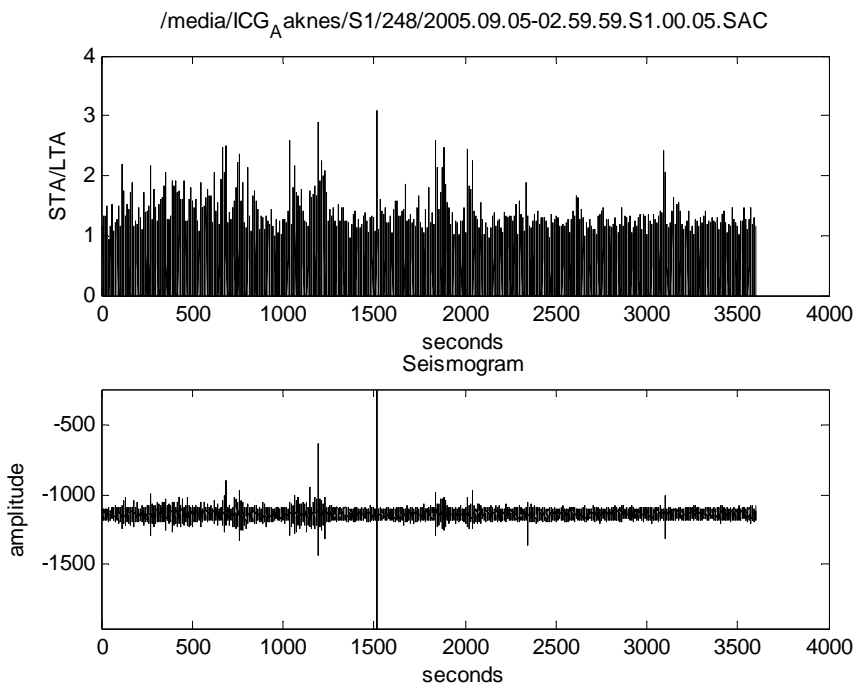
Figure 2.2: Example of data with little noise. The spike in the seismogram could be a microseismic event. The upper part is the STA/LTA calculated for each sampling point during one hour.

20
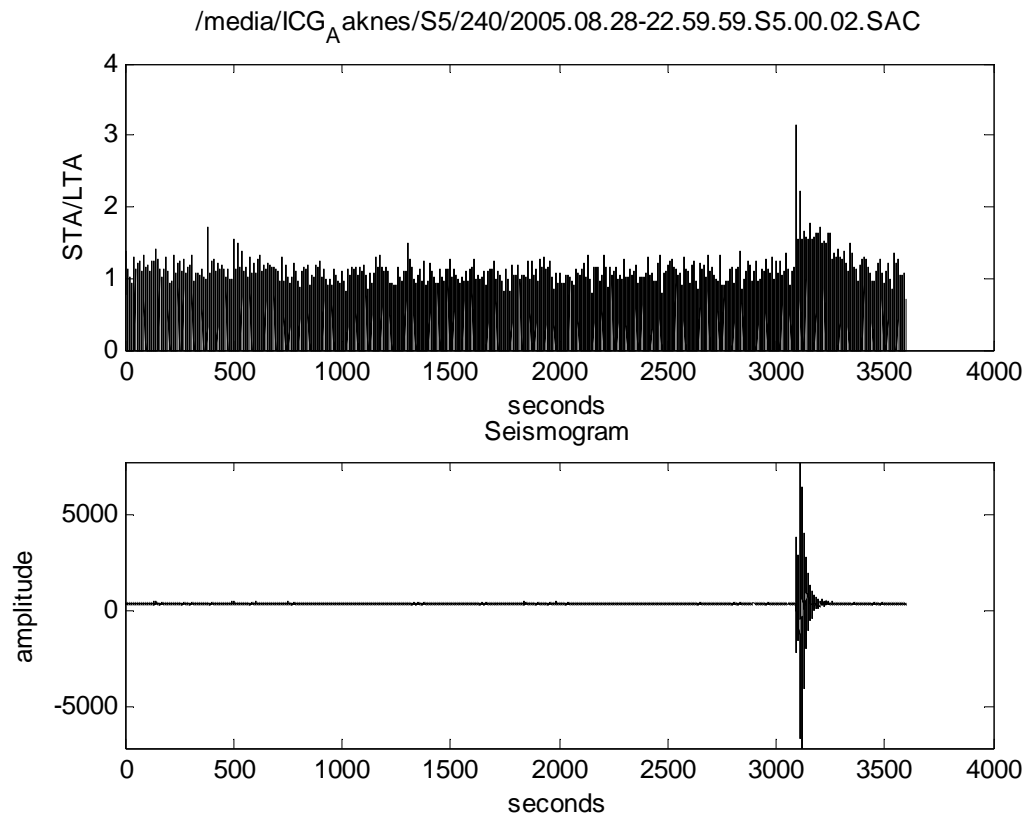
Figure 2.3: Example showing that the method also register local events.

This event is discribed in more detail under section 2.2.4: Results.

Part 3) The program findevents.m was run on the whole set of available sac-files (not the daytime). The run was controlled by script files and took approximately 8 x 24 hours to complete. Not all stations recorded successfully during the whole period of the experiment. Overall most of the stations were recording in the beginning but towards the end over half of the stations were out of order. An overview of the amount of data run in findevents.m and the list-names can be found in appendix B.1 (keep in mind that this is only for the hours during the night, the data from daytime can possibly exist, on the days were the data from the nighttime does not exist). The output of this process are files, called "found", that contains information about triggering of the STA/LTA algorithm in the corresponding data-files. Appendix A.3 and A.4 shows the scripts used to run findevents.m.

Part 4) The STA/LTA triggers on many features in the data which are not seismic events. This is done on purpose, to make sure no target events are missing out. Now some criteria had

to be set to sort out the real events from all that was detected up to this point. These criteria were:

1) For triggers on different components to be associated to the same event the time difference between the starting times of the triggers had to be less than 100 sampling points, which is the same as 400msec. (The maximum distance between two components is 100m, so with any possible velocity the waves will reach the next component within 400msec).
2) The event had to be registered on at least four of the components in one station, including the three components of the 3-C geophone.
3) The event had to be registered on at least two stations.

The found-files were gone through manually and for each time an event occurred on more than four components on the same station, it was registered in a list. This resulted in the list, of 93 events that can be found in appendix B.2. Going through this list, it turned out that 8 events were registered one more than one station.

2.2: The detected events

The 8 events have been numbered from 1 to 8 and their recordings on selected components are shown in figure 2.4 to 2.12. I have selected to display the components with the best signal to noise ratio. Appendix B.2 shows the exact time and day for the eight events, and where it is registered. In all, data from 50 days have been gone through, from August 28th to October 17th. If all stations had successfully recorded for the whole period, it would have given 49500 sac-files to scan (9 components on 10 stations for 50 days (11 hours during night time)). Of these were 28278 sac-files scanned, showing a recording rate of 57%.

Event nr 1 is not a micro seismic event from Åknes area, but a very nice local earthquake with duration of 120 s. It is a strong event with clear P- and S-wave arrivals and it is recorded at all operational components on all stations on the 28th of August. I have picked arrival times for the P- and S- phase and estimated the distance to the source of the earthquake using the equations 5 to 10. Equation 10 is a simplified version of equation 9, which is derived from the equations 5 to 8. From equation 10, which says that the difference between

the arrivaltimes of the p- and s-waves times 8 is equal to epicentral distance in km, I have calculated the average epicentral distance from the stations to be 137km.

$$Epicentral\ distance = \alpha T_\alpha \qquad \text{(Equation 5)}$$

$$Epicentral\ distance = \beta T_\beta \qquad \text{(Equation 6)}$$

$$T_\alpha = T_{\alpha\alpha} \quad T_0 \qquad \text{(Equation 7)}$$

$$T_\beta = T_{\beta\alpha} - T_0 \qquad \text{(Equation 8)}$$

$$Epicentral\ distance = (T_{\beta\alpha} - T_{\alpha\alpha})\frac{\alpha\beta}{\alpha - \beta} \qquad \text{(Equation 9)}$$

$$Epicentral\ distance = (T_{\beta\alpha} - T_{\alpha\alpha})8 \qquad \text{(Equation 10)}$$

Where α is the p-wave velocity, β is the S-wave velocity, T_α is the traveltime for the p-wave from the source to the geophone, T_β is the traveltime for the s-wave from source to geophone, $T_{\alpha a}$ is the arrivaltime for the p-wave, $T_{\beta a}$ is the arrivaltime for the s-wave and T_0 is the origin time of the earthquake. The value 8 in equation 10 is what is regularly used for earth continental crust. It was a bit difficult to pick accurate arrivaltimes, but I found that the event was closest to the stations S1, S2 and S4, and furthest away from stations S6 and S7. This indicates that the source is in a NE direction. A close-up of event nr 1 is given in figure 2.4.
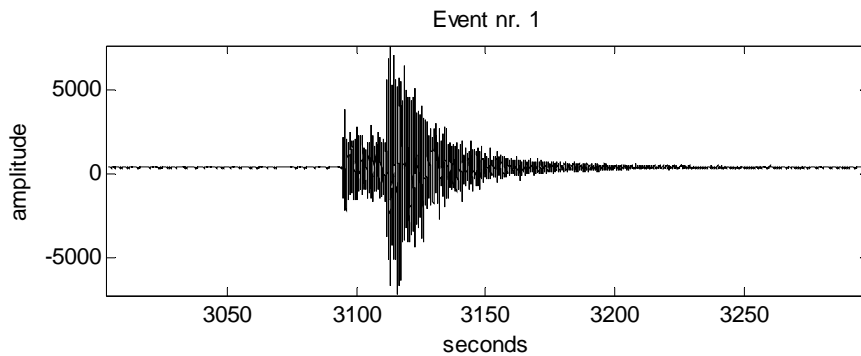
Figure 2.4: Event nr. 1 with a duration of 120 s. This is from the trace with best signal to noise ratio, component S6-3 . Registered on all operational components on all stations. This is a close-up of sac-file, recorded by component 2 at station S5, with starting time:2005.08.28-25.59.59.

Figure 2.5 shows event nr 2, which is a microseismic event with a duration of 1.6 s. The event is registered on station 5, 6, 7, 8 and 9. It was registered 30th of August. It is exactly the kind of event we have been looking. Figure 2.13 shows the waveforms on all components at station S7. For this event first arrival times has been picked and it has been localized (see chapter 2.4). An example of the picking procidure can be found in appendix C.10.
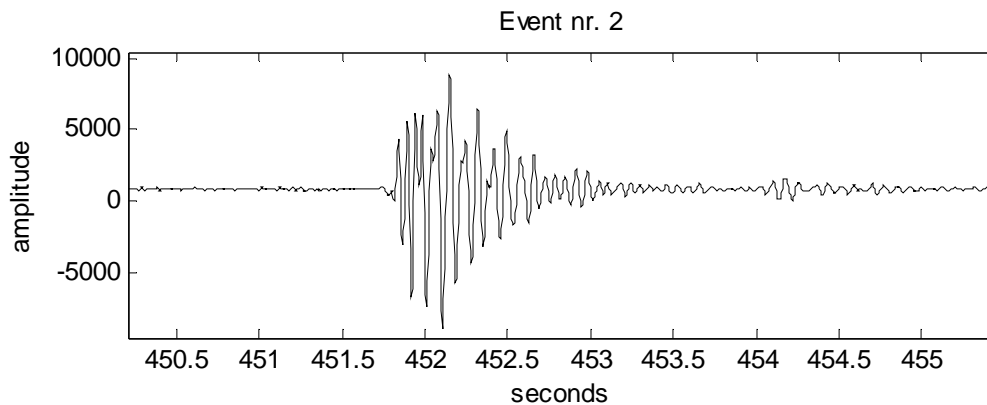
Figure 2.5: Event nr 2 with a duration of about 1,6 s, registered on most of the components at stations S5 to S9. It has not a clear P- and S-phase, but it has been localized by picking first arrivals. This was recorded by component 8 at station S7
Starting time of sac-file: 2005.08.30-21.59.59.

Figure 2.6 shows event nr 3, which is registered on station 5, 6, 7, 8 and 9 on the 4th of September, and it has a duration of 3.2 s. Figure 2.14 shows the waveforms for all the components at station S6. For this event, first arrivaltimes has been picked and it has been localized.
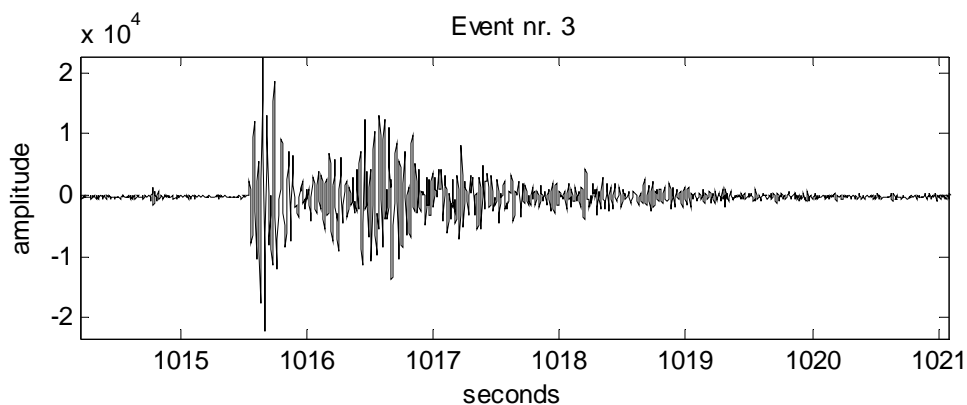
Figure 2.6: Event nr 3 with a duration of 3.2 s, registered on most of the components at stations S5 to S9. This was recorded by component 5 at station S8
Starting time of sac-file: 2005.09.04-21.59.59.

Figure 2.7 shows event nr. 4, which is only registered on station 1 and 2 on September 5th. It has a duration of 1.2 s. Figure 2.15 shows the waveforms for all the components at station S2. This microseismic event has also been localized.
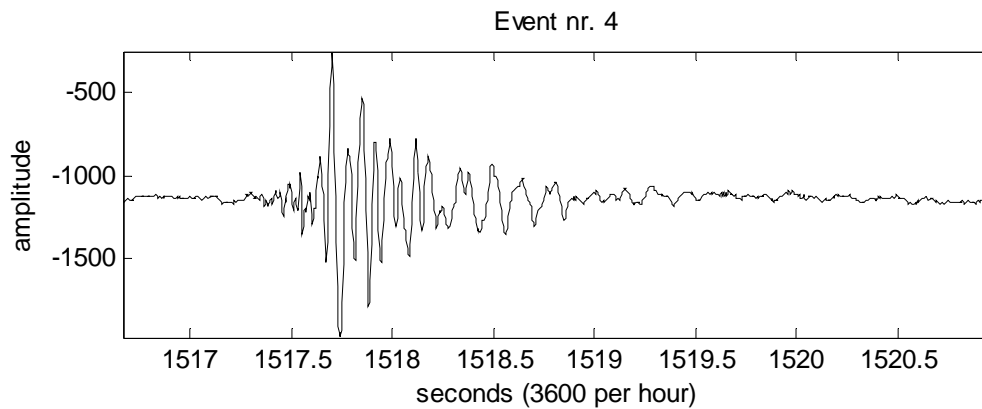
Figure 2.7 Event nr 4 with a duration of 1.2 s, registered on four components at station S1 and all components at S2. This was recorded by component 5 at station S2 Starting time of sac-file: 2005.09.05-02.59.59.

Figure 2.8 shows event nr 5, which is also registered on September 5th by station 1, 2 and 4. It has a duration of 1.6 s. Figure 2.16 shows the waveforms from all the components at station S2. This is a microseismic event, and it has been localized.
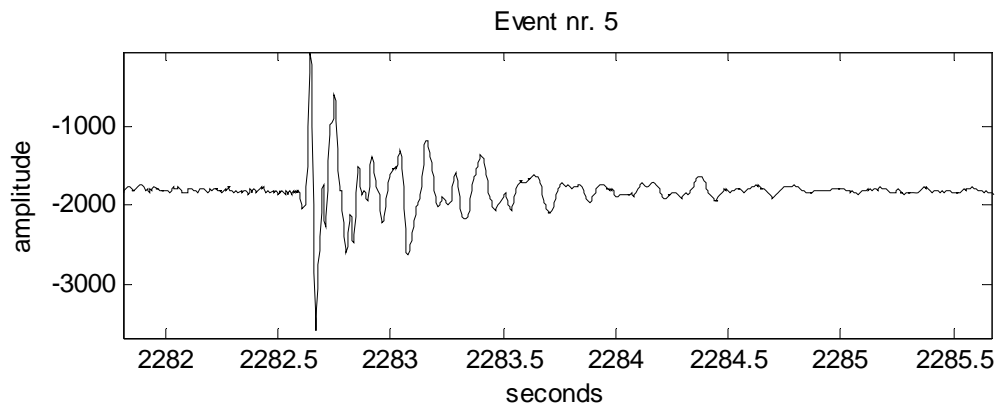
Figure 2.8: Event nr 5 with a duration of 1.6 s, registered on most of the components at stations S1, S2 and S4. This was recorded by component 0 at station S1 Starting time of sac-file: 2005.09.05-05.59.59.

Figure 2.9 shows event nr. 6, which is registered on station S1 and S6 the 10th of September. It is a clear event with a high signal to noise ratio, with duration of about 30 s. But it has no

clear onset, so I have not tried to localize it because picking arrival times was difficult. Figure 2.17 shows the waveforms from all the components at station S6.
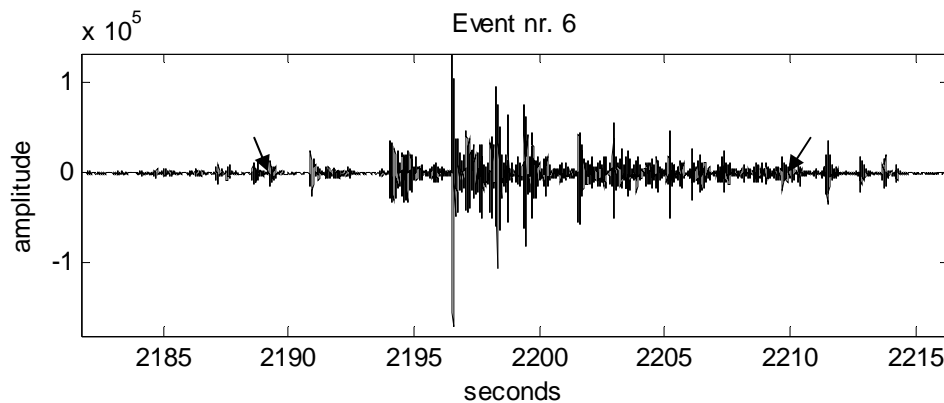
Figure 2.9: This is event nr 6. Duration between the two black arrows in the figure is 30 s. It is registered on almost all the components on station S1 and S6. This was recorded by component 4 at station S6. Starting time of sac-file: 2005.09.10-06.59.59.

Event nr 7 and 8 were registered on 15th of October. They were registered on most of the components at station S4 and S5, but they are also registered, though a bit weaker, at station S10. The two events are somehow related because they are the first two of five events in a series with decreasing amplitude. Only the first two have been strong enough to be registered by the algorithm for finding events. The five events are shown in figure 2.10. The time span from the first to the last is about 90sec. A close-up of event nr 7 and 8 is shown in figure 2.11 and 2.12. Both event nr 7 and 8 has a very short duration. They have a clear onset. I have tried to localize both of them. The waveforms, for both events nr. 7 and 8, from all the components at station S4 and S5 can be found in Figure 2.18 to 2.21. By looking at the wave forms it is very clear that the arrival times at the geophones for events 7 and 8 are much more different than for the other events. This is explained more closely and quantified in section 4.3.

Events 7 and 8
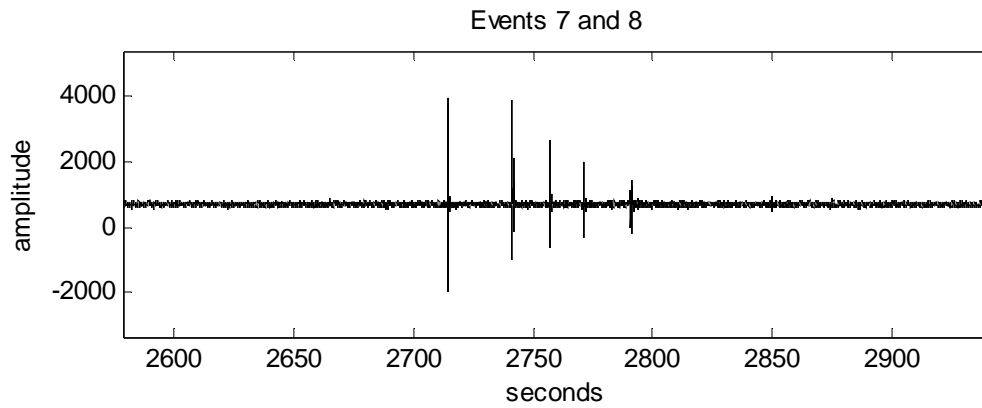
Figure 2.10: The five related events which occurs over a time-span of 90 s. The first two are events nr 7 and nr 8. This has been registered on most of the components at station S4 an S5, but also on some components at station S10. This was recorded by component 4 at station S4 Starting time of sac-file: 2005.10.15-06.59.59.
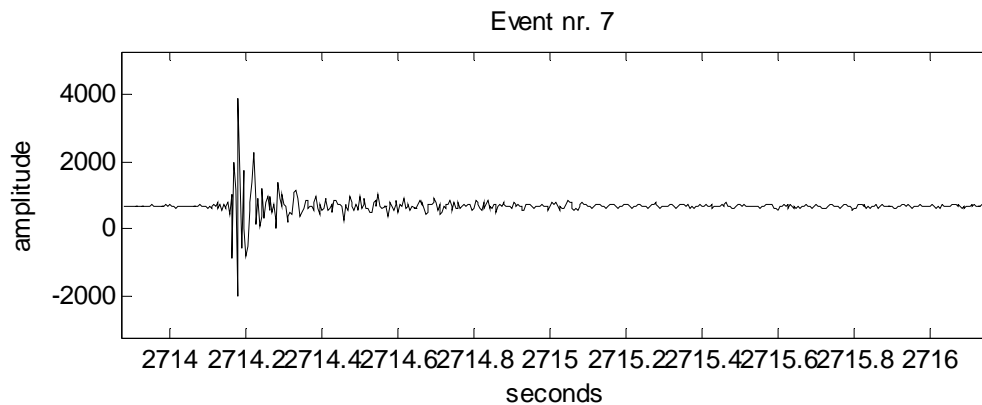
Event nr. 7


Figure 2.11: Event nr 7, the first in a serie of five events. It has a duration of 0.8 s. This is from the same file as figure 2.10 and 2.12.
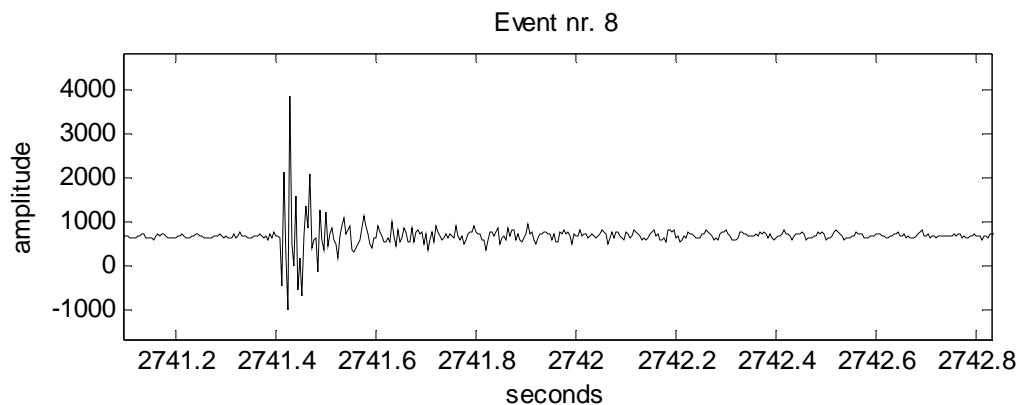
Event nr. 8

Figure 2.12: Event nr 8, the second in a serie of five. The duration is about 0.8 s. This is from the same file as figure 2.10 and 2.11.
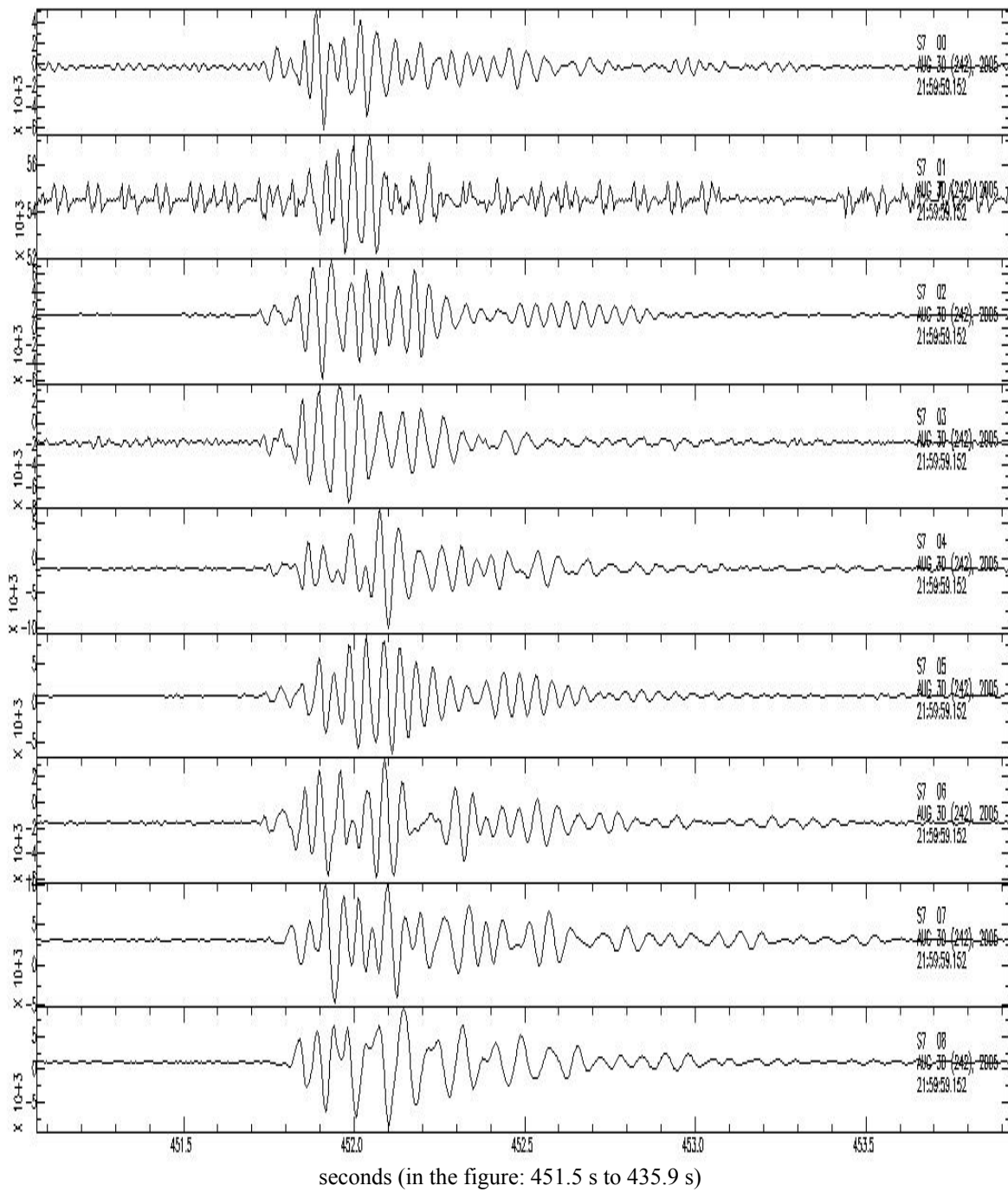
Figure 2.13: Waveforms for event nr. 2, at all the components in station S7.

seconds (in the figure: 451.5 s to 435.9 s)

28
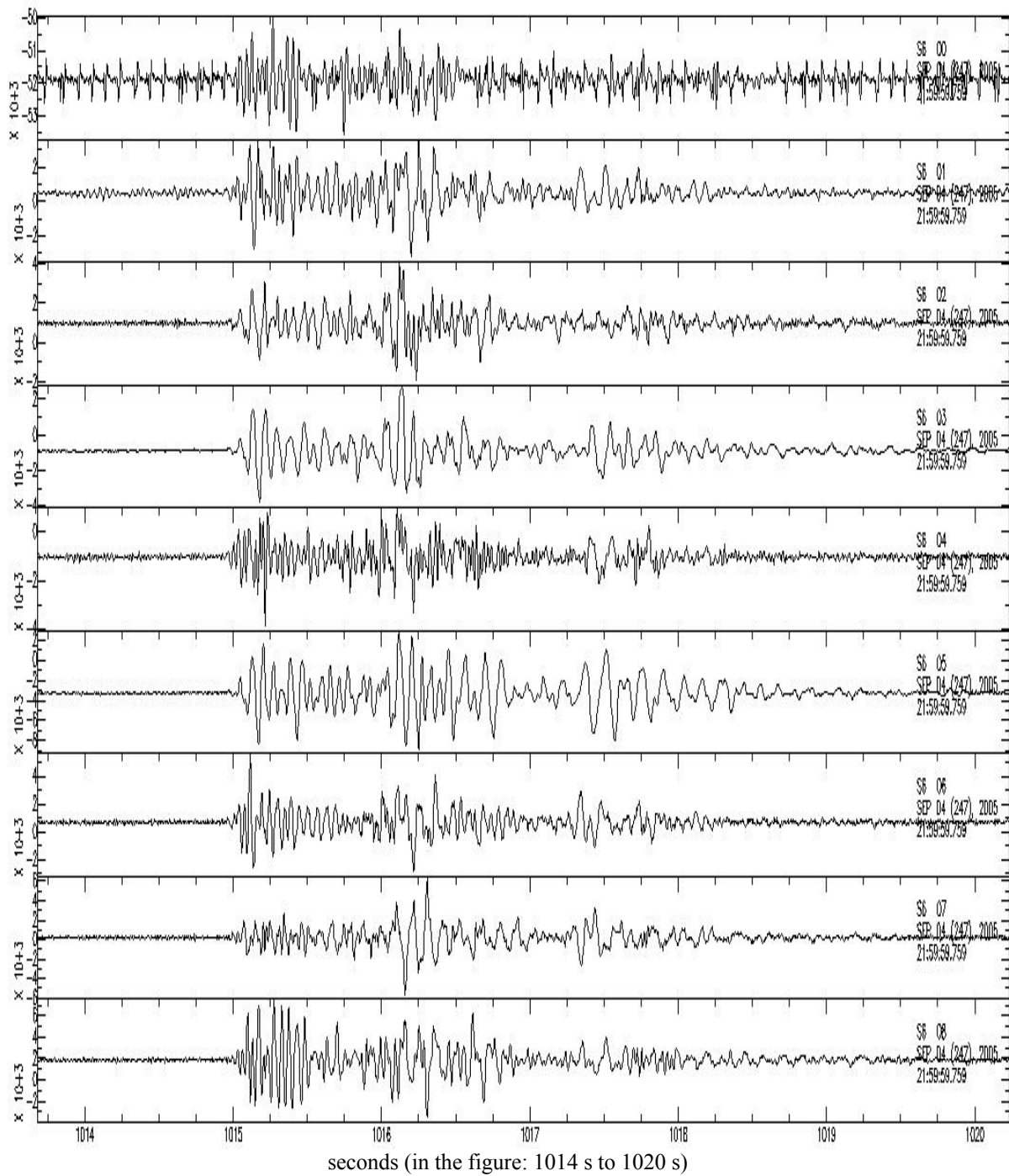
Figure 2.14: Event nr. 3. Waveforms from all the components at station S6
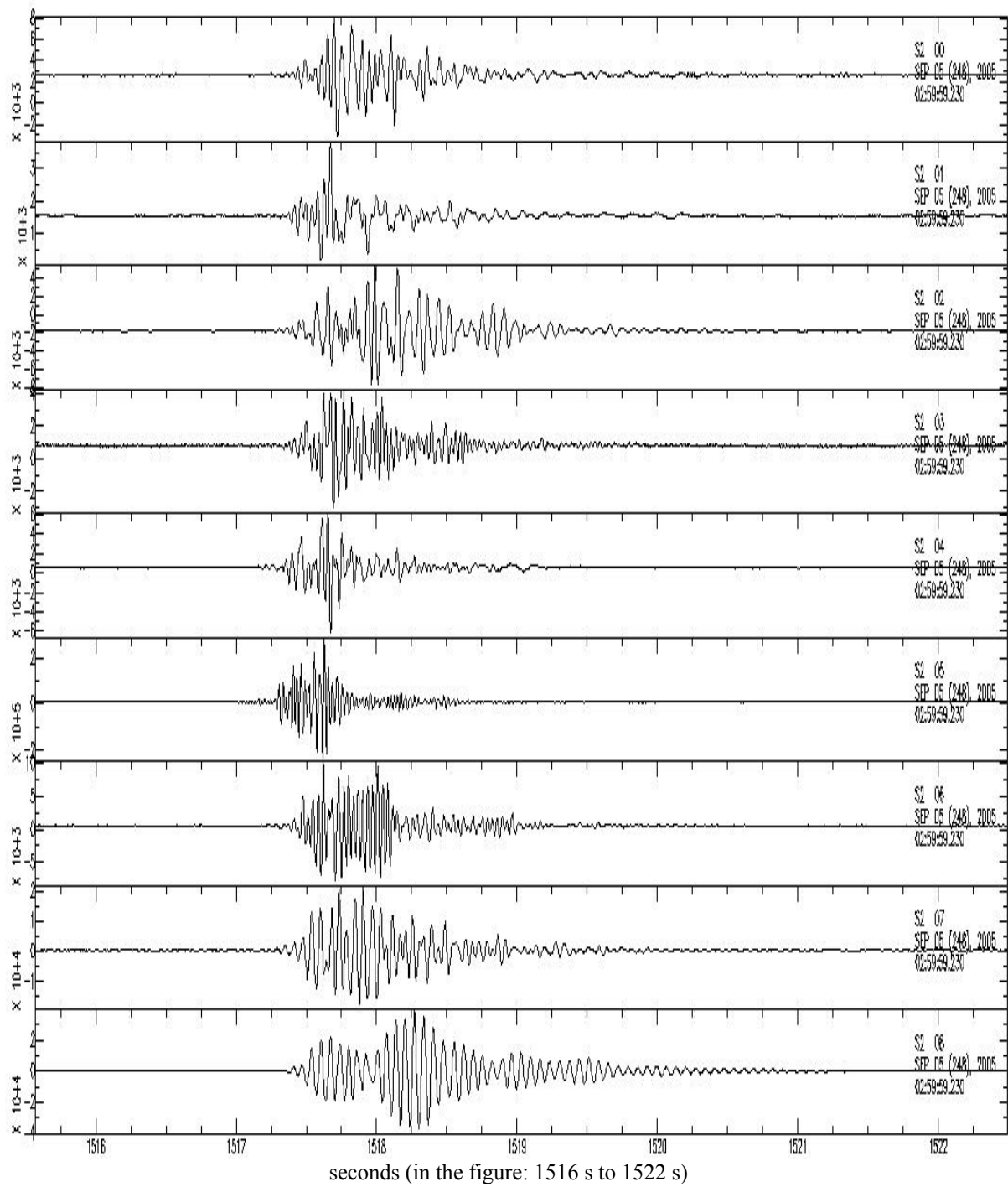
Figure 2.15: Event nr. 4. Waveforms from all the components at station S2.
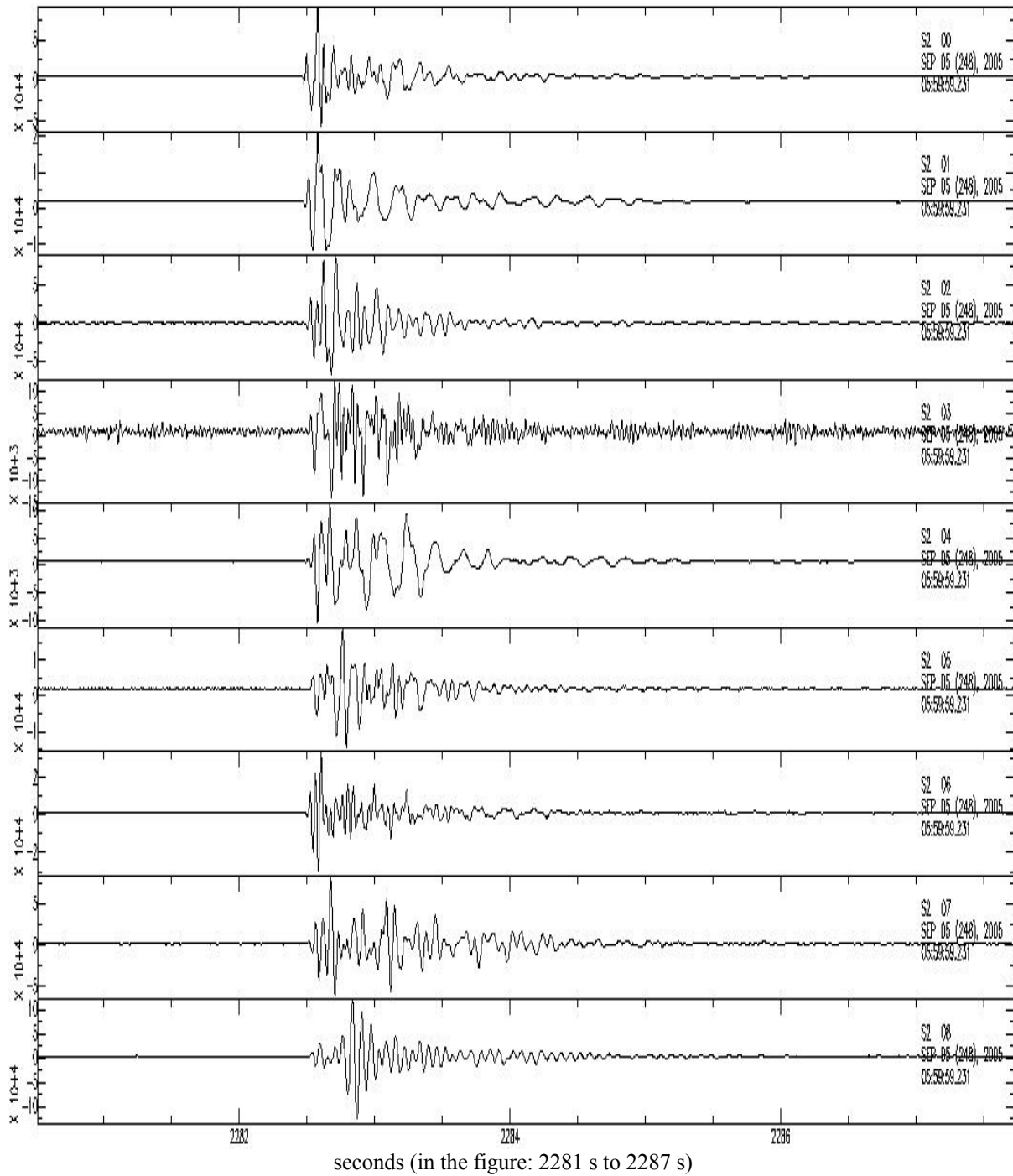
Figure 2.16: Events nr. 5. Waveforms from all the components at station S2.
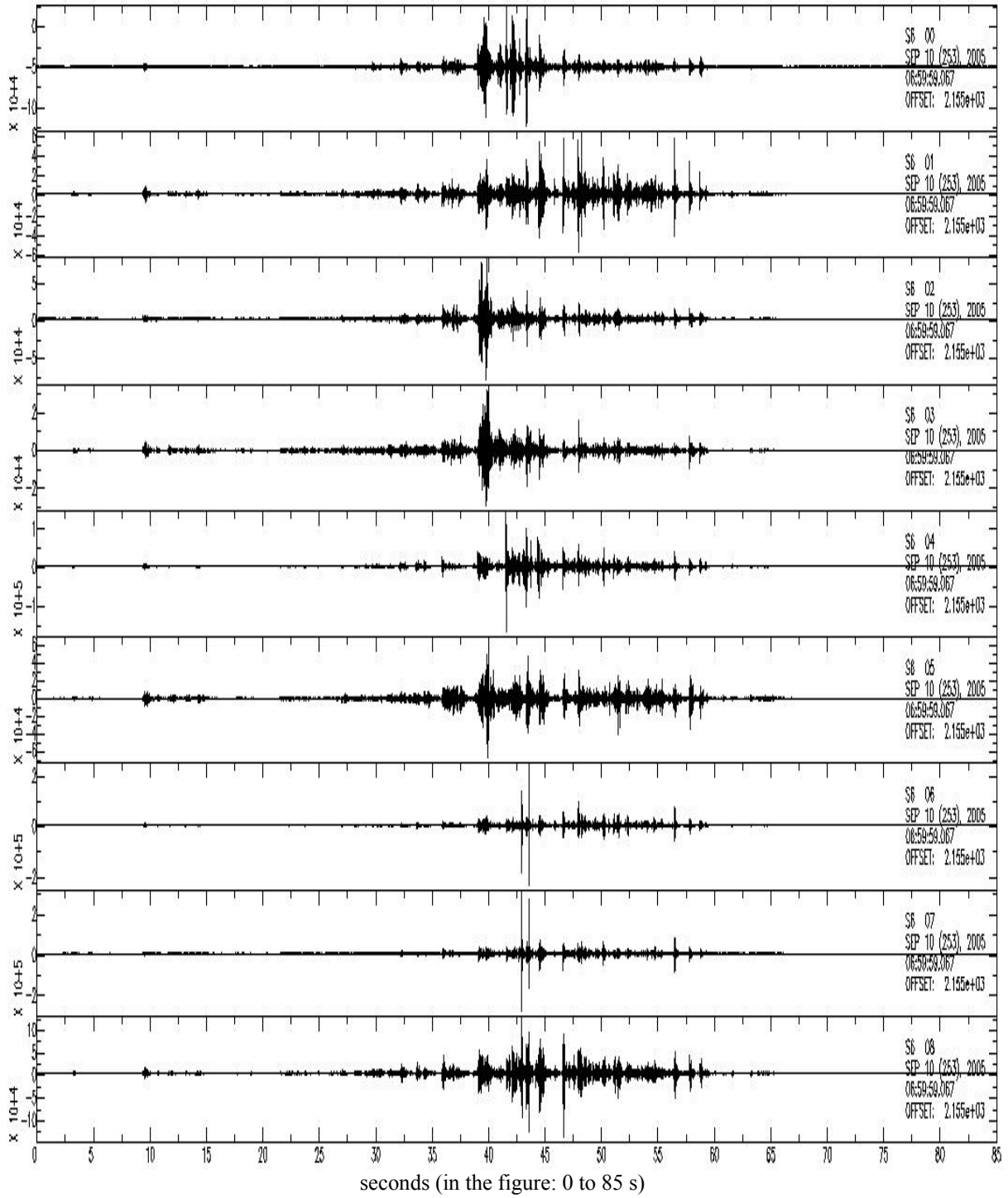
Figure 2.17: Event nr. 6. Waveforms from all the components at station S6.
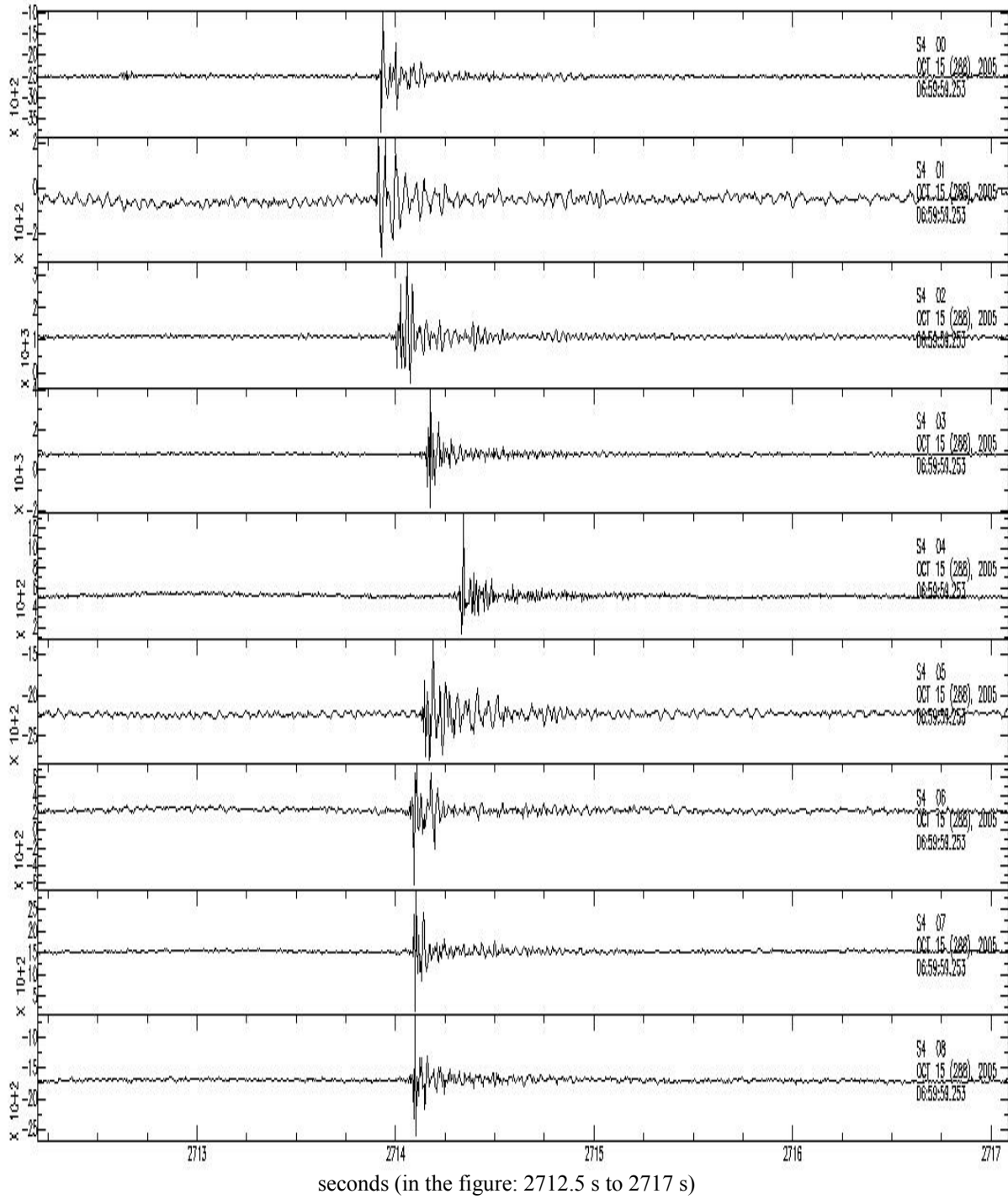
Figure 2.18: Event nr. 7. Waveforms from all the comopnents at station S4.
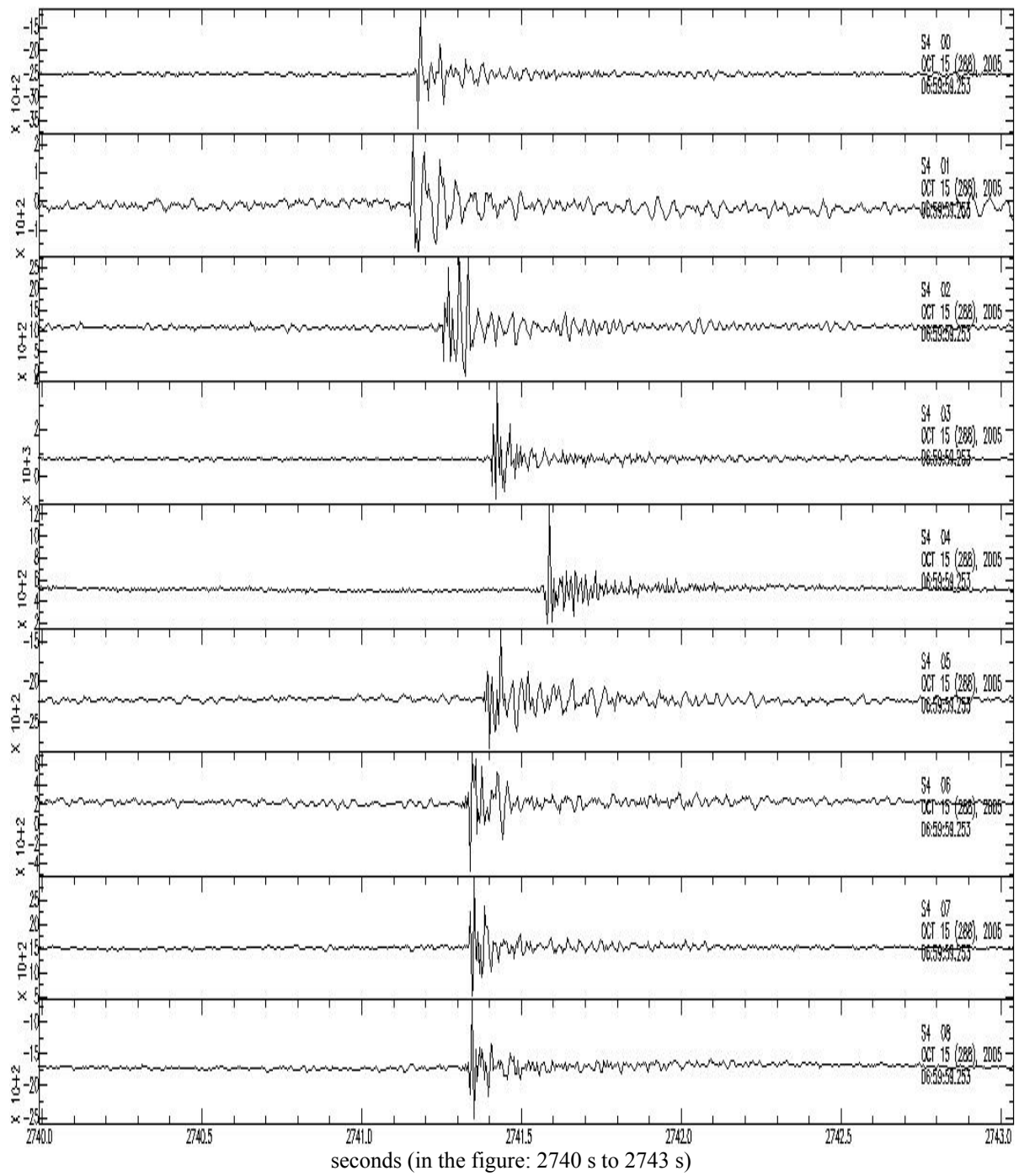
Figure 2.19: Event nr. 8. Waveforms from all the components at station S4.
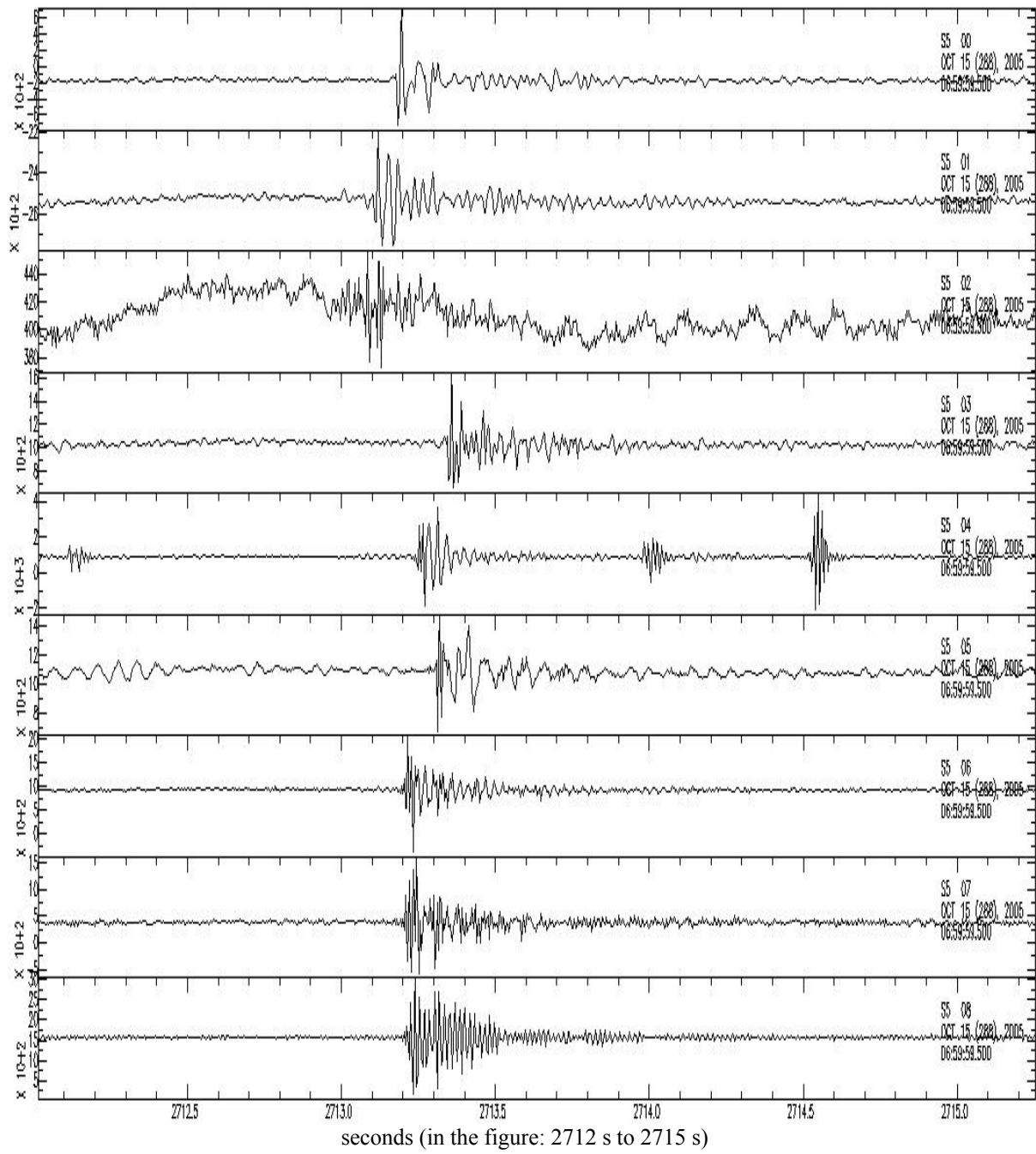
Figure 2.20: Event nr. 7. Waveforms from all the components at station S5.
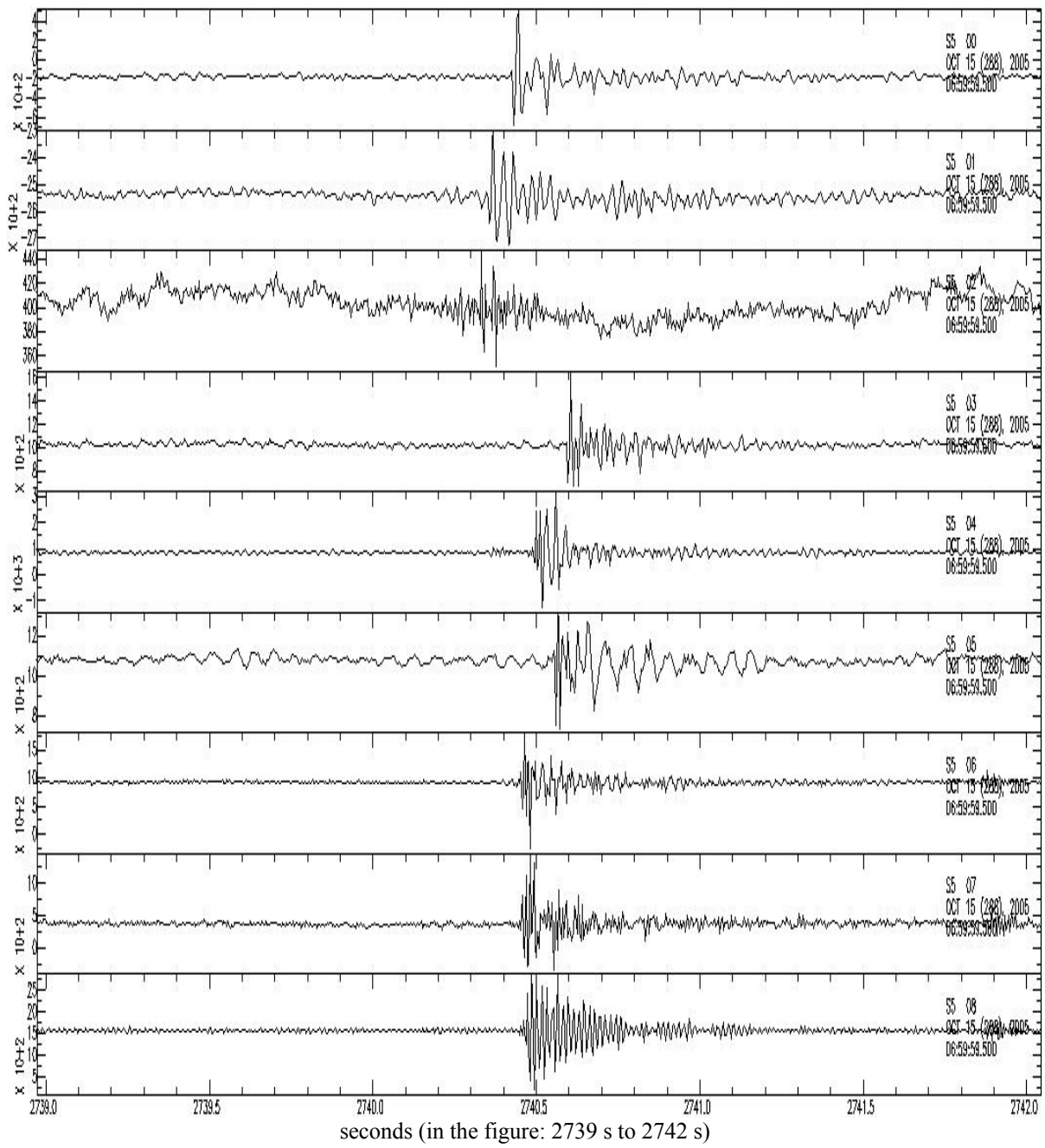
Figure 2.21: Event nr. 8. Waveforms from all the components at station S5.

3: VELOCITY MODEL

3.1: Travel time-distance plot from dynamite blasts

We are interested in finding positions of seismic events or the distance from receiver to source. All the information we have is the arrivaltimes at geophones at the surface. What we need is a relation between the epicentral distances and the traveltimes. This is traditionaly obtained by building a velocity model and calculating the traveltimes in this model. But there is another option: if we have recorded signals from a source with known position and origin time, both traveltimes and distances from that source can be calculated. A plot of traveltimes versus distances to the source provides us with the relationship between these two parameters, which we need for localizing other sources.

Figure 3.1: *The position of the seismic refraction profile (Dietrich etal., 2006).*

During the last two recording days (16th and 17th of October) of the temporary passive seismic IHR network (with which I have been working), a seismic refraction survey was done. The location of the line of receivers is shown in figure 3.1. Five dynamite blasts were used as a source in the refraction survey. The times and the positions of these blasts are known, and they were all recorded very clearly on all operational geophones at all stations in the IHR network (which more or less covers the whole slide area). The positions of the five blasts are shown in figure 1.6 and 4.4, where they are marked SP1 to SP5 in blue. SP is short for Shot Point. Appendix B.3 gives their coordinates and time. By using the information on the five shots together with arrivaltimes picked at the geophones, I have calculated traveltimes and plotted them together with their corresponding source-receiver distances in a

distance-traveltime plot. This gives an average relation between traveltimes and epicentral distance throughout the area.

For all the shots, first arrivaltimes was picked on most components with an uncertainty of 4msec. In appendix B.5, the arrivaltimes picked for all the shots are displayed. Appendix C display an example on how I have done the picking. From the positions of the shots (Appendix B.3) and the positions of the components (Appendix B.4) the direct distances between the shots and the components have been calculated by using equation 11 (Frery, 2007). The traveltimes were then calculated using the equation 12. Appendix A.5 shows the program made to do the calculations which was named findvelSPall.m.

$$Distance = \sqrt{(E_{SP} - E_R)^2 + (N_{SP} - N_R)^2 + (Z_{SP} - Z_R)^2} \qquad \text{(Equation 11)}$$

$$traveltime = picked\ arrivaltimes - time\ of\ shot \qquad \text{(Equation 12)}$$

E is the easting in meters, N is the northing in meters and Z is the elevation. A distance versus traveltime plot was made. Figure 3.2 and 3.3 shows all the traveltimes plotted versus. the distances from the source.
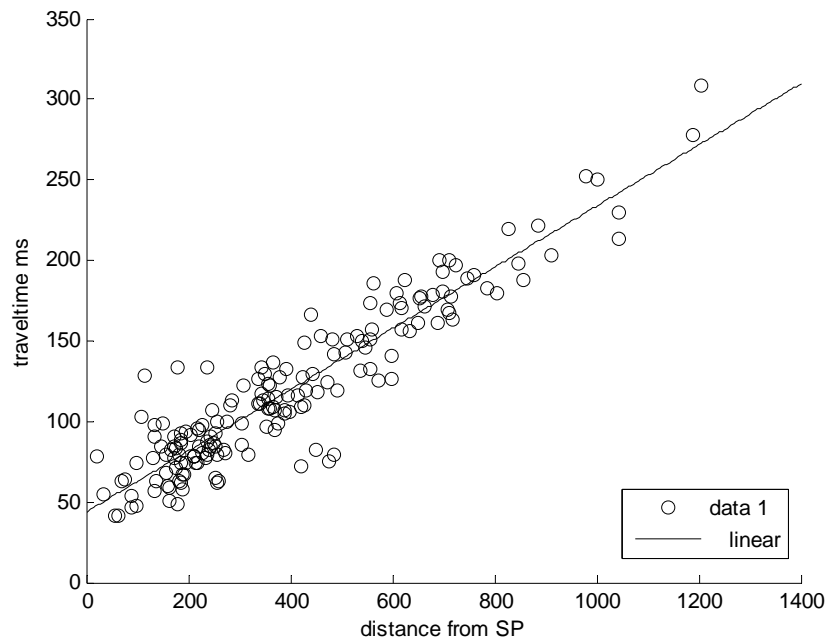
Figure 3.2: The traveltime-distance plot for all the picked arrival times.
The solid line is a least square linear trend.
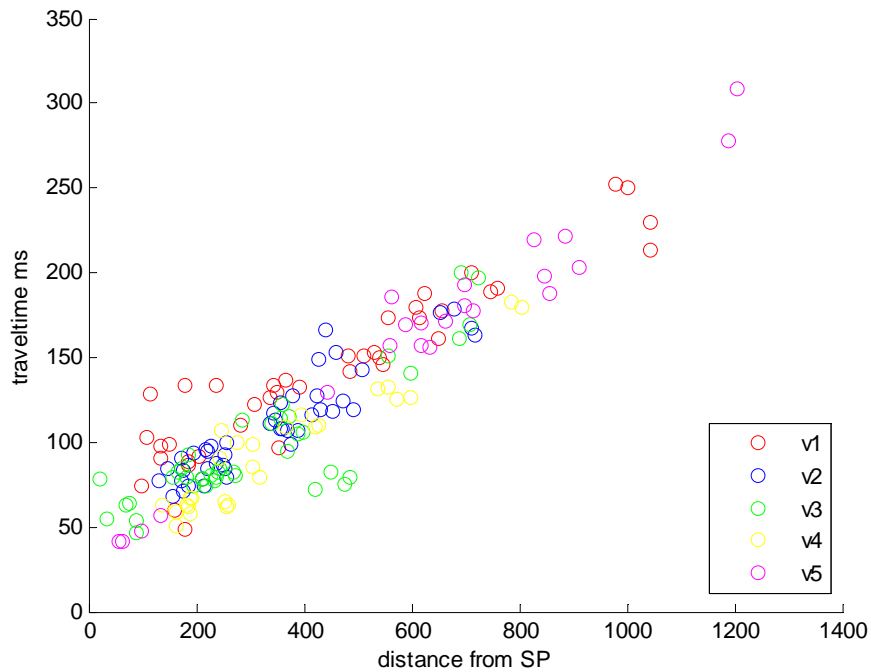
Figure 3.3: Traveltime-distance plot for all the picked arrival times.
The different colours represent arrival times for the five shots,
v1 is for SP1, v2 is for SP2 and so on.

Figure 3.3 shows the travel times in the traveltime-distance plot with traveltimes for each of the shots plotted with different colours, labelled from v1 to v5 (for the shots SP1 to SP5 respectively). The plot shows that all the arrivaltimes fall on the same trend within a certain range, except for some outliers from SP1 and SP3. The outliers could result from bad picking. I have chosen to use a linear trend calculated from all the traveltimes together to find the relation between traveltime and epicentral distance. The linear trend in figure 3.2 is found automatically in Matlab by a least-squares method. The slope of the traveltime-distance curve (also called t-x diagram) corresponds to the slowness of the waves (Musset & Khan, 2000). The trend in figure 3.2 follows equation 13.

$$\text{Traveltime} = (\text{slowness X distance}) + T_{intercept} \qquad \text{(Equation 13)}$$

The slowness is 0.19 ms/m and the $T_{intercept}$ is 43.737 ms. Equation 13 with the values of $T_{intercept}$ and slowness gives a relation between epicentral distances and traveltimes, which was what I wanted to find. The equation will be used in the localization process in chapter 4.

3.2: The velocity model

From the relation between traveltimes and epicentral distance a velocity model can be derived. Given the slowness equal to 0.19 we can find the velocity with equation 14.

$$\frac{1}{v} = 0,19 ms/m \Rightarrow V = \frac{1}{0.19 ms/m} = 5,26 km/s \qquad \text{(Equation 14)}$$

The linear trend in figure 3.2 does not intersect the time axis at zero. A timing error of the shots can cause a $T_{intercept}$ larger than zero if the real time of the shot has been delayed. Also if I have in general picked all the arrivaltimes later than when they actually arrived, the whole trend will move upwards in the t-x diagram, causing $T_{intercept}$ to be larger than zero. If the timing and picking are correct a $T_{intercept}$ larger than zero indicates the presence of a low velocity zone over a half space with a uniform velocity. In a t-x diagram, the direct wave following the surface will result in a line with a steep slope, starting at the origin and intersecting the next first arrival line. The slope of this line gives the slowness of the first layer; this together with $T_{intercept}$ can give the thickness of the surface layer (Musset & Khan, 2000). In the plot in figure 3.2 it is not possible to draw such a line from the plotted values so it is not possible to say how thick the first layer is or the velocity. It could be that none of the distances between shot point and component are short enough for the direct wave from the shot to arrive first. From this interpretation and the velocity found in equation 14 I can deduce that the velocity model is of the form shown in figure figure 3.4.
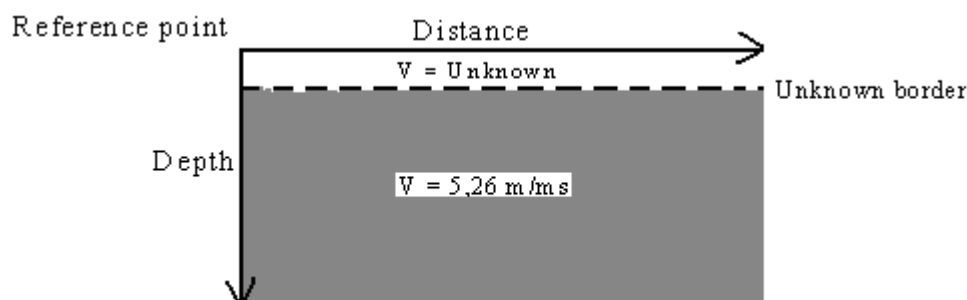
Figure 3.4: The velocity. The white layer on top is thin, but the velocity and thickness is unknown. The grey layer has a uniform velocity of 5.26 km/s

There is a thin layer at the surface with unknown velocity and unknown thickness. Below the surface layer there is a uniform half space with velocity of 5.26 km/s. I know that the whole

area consists of gneiss, which probably corresponds to the uniform half space with velocity 5.26 km/s. The thin surface layer could be gneiss that are heavily fractured, and thus have a low velocity. If some of the events found are so close to a component that the waves which travel through the surface layer arrives first, the result of the localization using this model can be a bit inaccurate.

The waves generated by the shots have of course also been recorded by the geophones which were deployed specially for the refraction survey. The geophones were located on a line along the slope of the Åknes site between the shots SP2 and SP4 (see Figure 3.1). The refraction data have been interpreted by Dietrich et al. (2006). The resulting velocities are shown in figure 3.5. I did not directly use the interpreted velocities from the refraction survey, because they are just for a profile in the middle of the area, and I need a velocity model for the whole area. Instead I have used the interpreted velocity model from the refraction profile, to control that the relation in equation 13 is a good estimation, by comparing it with my velocity model in figure 3.4 The interpreted velocity model from the refraction profile (in figure 3.5) gives two low velocity layers over a homogeneous half space with a constant velocity of 5.73 km/s (Dietrich etal., 2006). In my model I have one low velocity layer, with an unknown thickness and velocity, over a homogeneous half space with a velocity of 5.26 km/s. Though my model is not as detailed, the two models are not very different, and I conclude that my model is adequate for localization.

The velocity model in figure 3.5 is partly interpreted from the seismic section in figure 3.6. The seismic section can be compared to the t-x diagram in figure 3.2. The refraction line from the refraction survey intersects the time axis at a $T_{intercept}$ equal to 0.08 sec (80 ms). For the whole area, I found $T_{intercept}$ of about 44 ms (figure 3.2). Since this intercept is somehow proportional to the thickness of the low velocity upper layers, this could mean that in the area of the refraction profile, the low velocity zone at the surface is thicker than it is in average over the whole area.
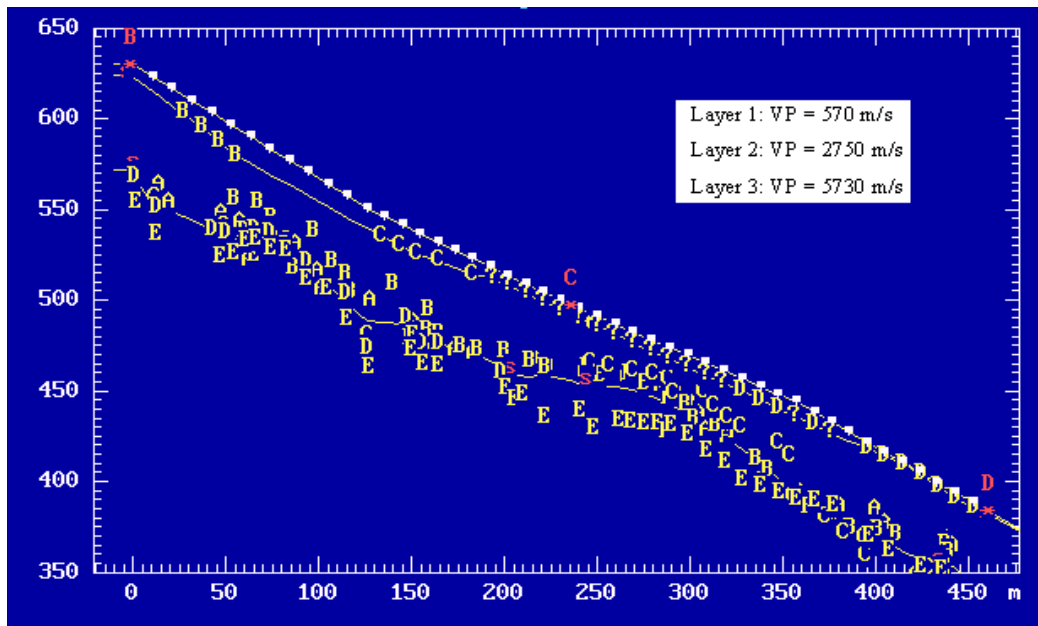
Figure 3.5: A vertical cut from the refraction profile. y-axis are elevation in meters and x-axis are horizontal distance from the starting point of the profile. In the white box are the interpreted velocities in three different layers. The yellow letters form A to E represents interpretation from the shots SP1 to SP5. The points B C, and D marked in red, are the end points of the shots SP2, SP3 and SP4. The white dots at the surface marks the receivers (Dietrich etal., 2006).
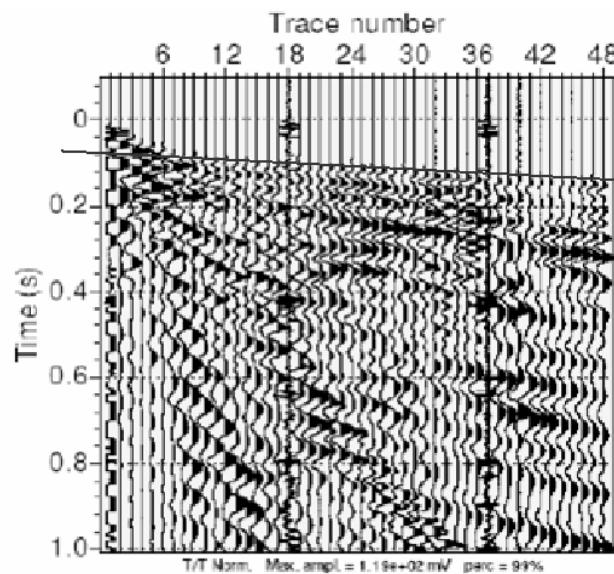
Figure 3.6: Seismic section from SP2 recorded in the refraction survey. This is some of the background from which the velocity model in figure 3.6 had been interpreted. Refraction line from the homogenous half space I have traced out with a solid line. (modified from Dietrich etal., 2006.)

What is shown in this paragraph is not important for the results of my work, but I have chosen to include it to show that different approaches have been tried out. I tested also the possibility of using a model with a velocity that varies linearly with depth. Figure 3.7 shows in different

colours the calculated distances versus traveltimes for five different gradients, varying from 0.0625 km/s to 0.1 km/s. For each gradient three different values of 0.5 km/s, 1.25 km/s and 2 km/s were also tested for the surface velocity. When comparing figure 3.7 with figure 3.2 showing the measured results, we see that none of the trends here fit the data. The traveltimes plotted in figure 3.3 should have fallen on one of the trends in figure 3.7 if a velocity model with a gradient would have been adequate. The conclusion is that a velocity model with a velocity that vary linearly with depth is not a good model and that a slow layer above a homogeneous half space is much more adequate.
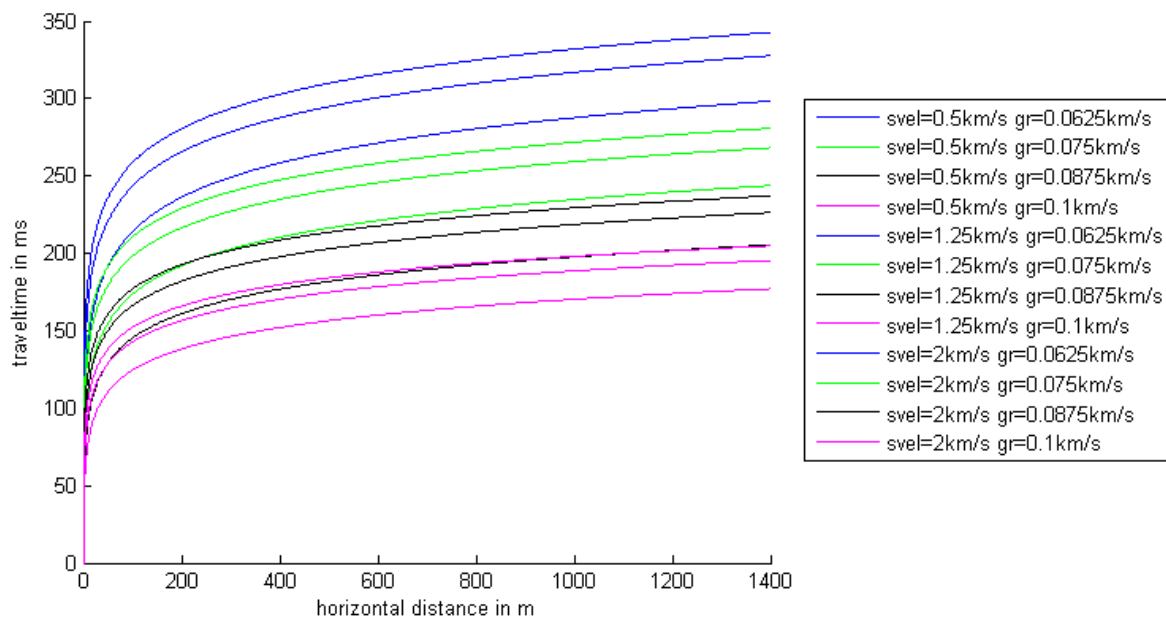
Figure 3.7: Traveltime vs. distance plot. The different colours correspond to different gradients, labelled "gr" in the legends. The three trends with the same colour have different surface velocity, labelled "svel" in the legend.

3.3: Uncertainty concerning the locations of the geophones

In the sac-files containing the data, the components are numbered from 0 to 8, and there is no information in the header on the location of the geophones, and no info on which of the nine components at a station is part of a 3-C geophone. The stations are in the data named S1 to S10. The information I have on the positions of the geophones is the same as used by Frery (2007). In this information the stations are labelled the same way, S1 to S10, as in the data, but the components are labelled 1 to 7 and the 3-C geophone is one of these 7 components (which one changes from station to station). I had therefore to identify which of my data files

belong to which component in Frery's table. In order to do that I compared the waveforms of the shots SP1 to SP5 in my data to those plotted by Frery in her report. The correspondence between the two numbering systems can be found in appendix B.5.

In many cases the data show that the last three components (nr. 6, 7 and 8) of a given station stand out as more similar than the other components. By looking at Appendix B.5, we see however that it is only at S2 and S4 that the 3 components of the 3C geophone are in the last three components. Three examples are shown in figure 3.8 to 3.10. The traces in figure 3.8 are from station S1; here the components in the 3C geophone should be components 3, 4 and 5. The traces in figure 3.9 are from station S3; here also the components 3, 4 and 5 should be those in the 3-C component geophone. In figure 3.10 traces from station S5 are shown; here the 3-C component geophone should have included components 1, 2 and 3. If the data mostly are a consequence of vibrations in the ground (whether it is vibrations from noise or seismic events), and not a consequence of electronic or instrumental interference, I would think that components in a 3-C geophone will experience somewhat the same vibrations (though in different directions). If this is correct I would further expect the seismic traces from the three components in the 3-C geophone to stand out as more similar to each other than the other 6 single-component geophones at the same station. If the similarities in the traces of component 6, 7 and 8 are only from instrumental or electronic noise, it could mean that the three last components are some how wired together but they could still be from different geophones. If this is the case, there are no problems concerning the geophones coordinates. The example which gives clearest reason for suspecting uncertainty of coordinates is figure 2.20 and 2.21. These figures shows that the arrival times (for S5) at the three last components are close to the same, while the other components have different arrival times. In S5 the three components in the 3-C geophone is supposed to be components 1, 2 and 3. First arrival times are always the same for all components in the same geophone.

This leaves some uncertainty concerning the exact location of the components, but fortunately only within one station, there is no uncertainty concerning to which station each component belongs. The uncertainty is max 100 m. If some components have a wrong location, this will move the points in figure 3.2 at the most 100 m along the x-axis. This leads then to some uncertainty in the travel time-distance formula (equation 13) and in the localization of the events, but since I know that the affiliation of the components to the stations are correct, this uncertainty is lower than the uncertainty of the arrival time picking

and the uncertainty of the method for making the velocity model itself. So the work on this thesis is not all a waste even if the positions turn out to be a bit wrong within a station.
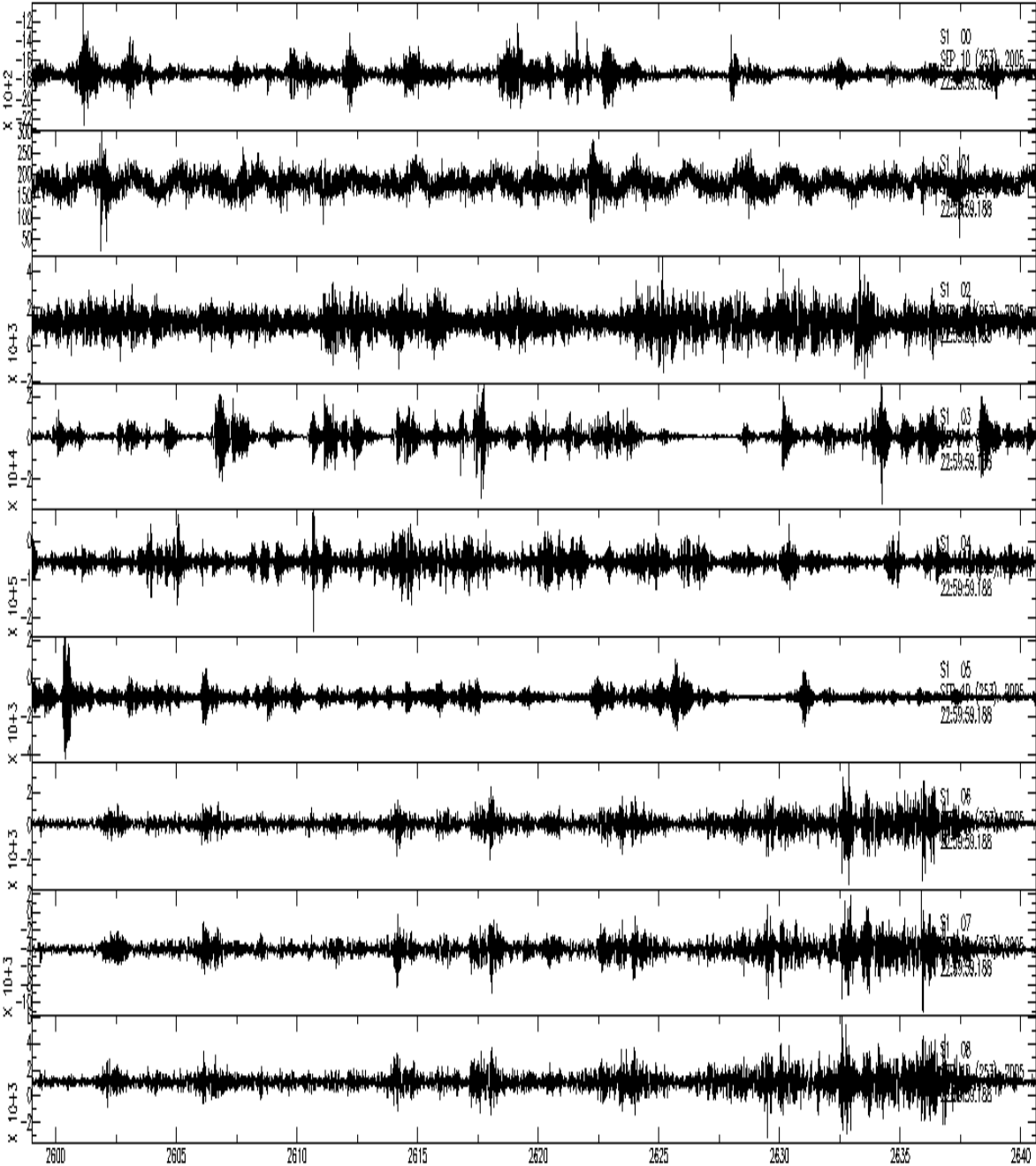
Figure 3.8: Traces from all the components at station S1. Components 3, 4 and 5 should comprise the 3C geophone. This is recorded on September 10th. The starting time of the sac-file is 22.59.59.
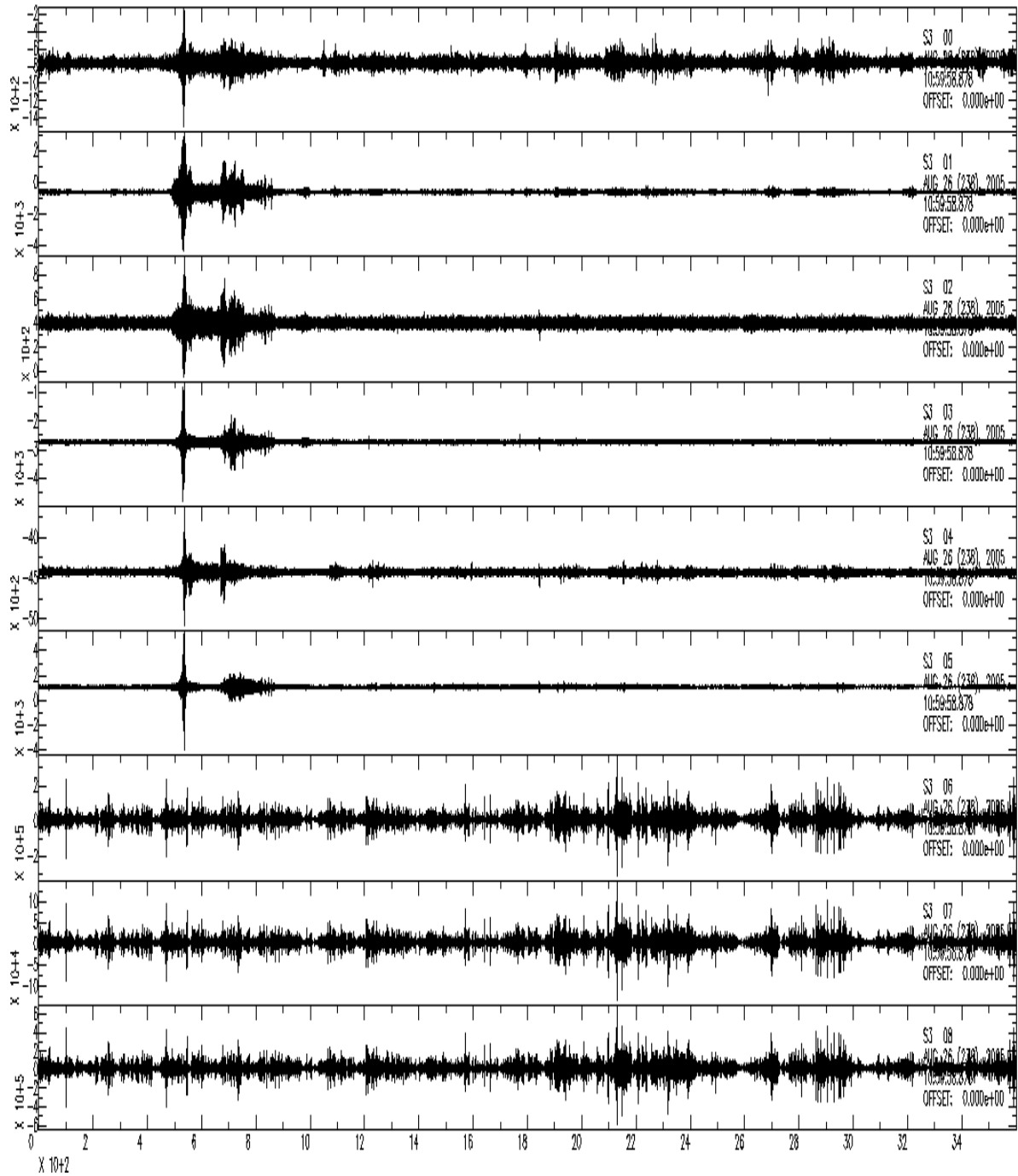
Figure 3.9: Traces from all the components at station S3. Components 3, 4 and 5 should be from the 3C geophone. This is recorded on August 26th. Starting time of the sac-file is 10.59.58.
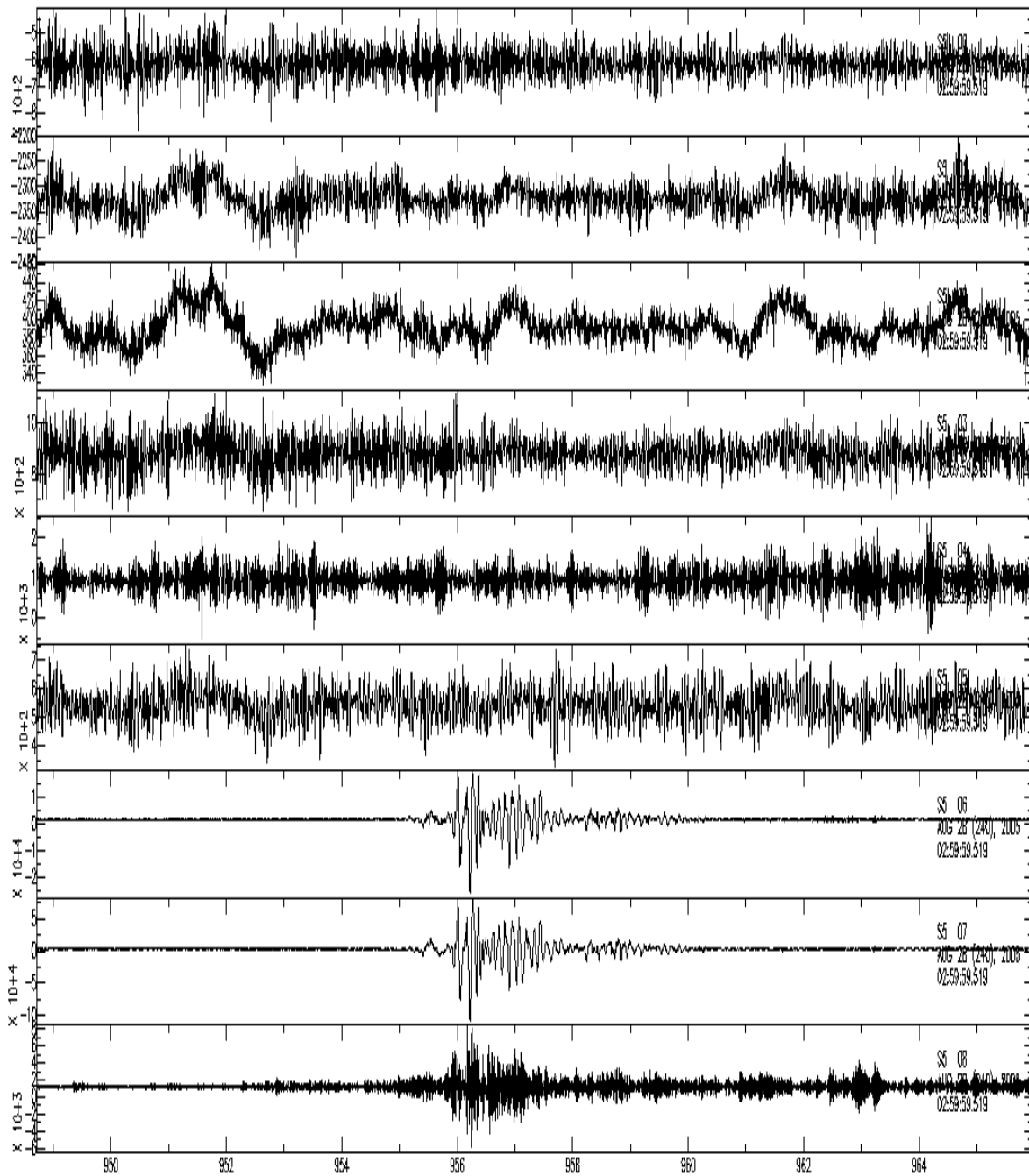
Figure 3.10: Traces from all the components at station S5. Components 1, 2 and 3 should be from the 3C geophone. This is recorded on August 28th. Starting time of sac-file is 02.59.59.

4: LOCALIZATION

Because of the uncertainty concerning the velocity model and that determimning an earthquakes hypocentre always is a trade off between depth and origin time of the source, it was chosen to only try to localize the epicentre of the microevents. That is location of the microearthquake on the slope, but not its depth. The localization was done with a misfit-function or an error function. What is done then is to make a grid of the slope and for each node in the grid calculate the traveltime to each of the components, using the traveltime function derived in chapter 3.1. For an event the error between the measured traveltime and the calculated traveltime is plotted in the grid for each node. I did not have the time of the microevent, so I had to calculate the misfit for different possible origin times to find the best t_0 (origin time of event).

4.1: Determination of the best slope plane

First I needed to find a coordinate system which is parallel to the slope, make a grid and convert all the components from E, N and altitude coordinates into the new grid. Finding a coordinate parallel to the slope requires a measure of the strike and dip of the slope. Strike and dip were first calculated for three pairs of components with the same altitude, to get an estimate on how much the new coordinate system needed to be rotated compared to the E, N, altitude system. The strike was calculated to be: 76°, 68° and 61° with an average of 68°. The dip was calculated to be: 52°, 30° and 36° with an average of 39°. Then the strike and dip were defined: The northernmost geophone, nr. 2 on station S1, was chosen to be the one at the vertical of a reference point in the rotated coordinate system (geophone nr 2 on the S1 station is named S1-3 in appendix B.4). Assuming that the geophones had not been placed systematically on hills or in small depressions, I define the reference plane as the one which would at best go through all the geophones. The geophones do not lie in one plane, and they will all have an "altitude" or a distance to a plane, but the best plane to use is one where the sum of all the "altitudes" is zero. The coordinates to all the components (relative to component S1-3) were rotated with different values for strike, dip and altitude of S1-3 from reference point. The strike was varied between 60° and 80°, the dip varied between 35° to 45°, and altitude from the reference point varied from -5 m to 5 m while the distances from

Strike = 72°

Dip = 35.9°

Distance from reference point = 4 m

The standard deviation was most sensitive to the value of dip.

4.2: Method for localization

The next step was to use the best slope plane and write an algorithm for localizing the microearthquakes on this plane. The program, lokalisering.m, that was written for the localization can be found in Appendix A.6. The first thing the program does is to rotate the coordinates of the geophones from East, North and altitude, according to the strike and dip with rotational matrixes shown in equation 16 and 17.

$$\begin{bmatrix} X' \\ Y' \\ Z' \end{bmatrix} = \begin{bmatrix} \cos\alpha & -\sin\alpha & 0 \\ \sin\alpha & \cos\alpha & 0 \\ 0 & 0 & 1 \end{bmatrix} \begin{bmatrix} E \\ N \\ elevation \end{bmatrix} \qquad \text{(Equation 15)}$$

$$\begin{bmatrix} X \\ Y \\ Z \end{bmatrix} = \begin{bmatrix} \cos\beta & 0 & -\sin\beta \\ 0 & 1 & 0 \\ \sin\beta & 0 & \cos\beta \end{bmatrix} \begin{bmatrix} X' \\ Y' \\ Z' \end{bmatrix} \qquad \text{(Equation 16)}$$

Where X', Y' and Z' are the new coordinates rotated horizontally according to the strike, α, and X, Y and Z are the new coordinates rotated according to dip, β. The cell size in the grid is 20 m x 20 m. The distance along slope (omitting z) between the geophone and a node in the grid is then calculated using equation 18.

$$distance = \sqrt{(X_n - X_v)^2 + (Y_n - Y_v)^2} \qquad \text{(Equation 17)}$$

Where index n indicates node and c indicates geophone. The theoretical traveltime from that node to the geophone can then be calculated by using equation 19. Which is the relation found in section 3.1.

$$theoretical\ traveltime = T_{intercept} + slowness \times distance$$

(Equation 18)

Were $T_{intercept}$ is the intersection point between traveltime curve and traveltime axis in the traveltime-distance plot. $T_{intercept} = 44$ ms, slowness $= 0.19$ ms/m. I have picked the arrival times at the different components but in order to calculate the measured traveltimes, I need to calculate the origin time t_0 of the microevent. This is done by using equation 20.

$$measured\ traveltime = arrivaltime - t_0$$

(Equation 19)

In order to evaluate it, I calculate misfit functions with different values for t_0, varying from 0 to 120ms before the first arrival. Finally the misfits from all components at each node are summed up. The misfits are calculated by using equation 21.

$$misfit = (measured\ traveltime - theoretical\ traveltime)^2$$

(Equation 20)

The misfit is plotted with a contour plot. The nodes with the lowest misfit are thought to be the location of the microevent. The calculations in equations 18 to 21 was tested for different values of t_0 and plotted. To learn how the algorithm behaves, this was tested out on the five active shots, SP1 to SP5, because here we know the exact location and time. Figure 4.1 to 4.3 shows the result of the localization of SP2 using three different values for t_0. I have also plotted the locations of the stations S1 to S10 but omitted their numbers for clarity of the figure. The locations of the five shots SP1 to SP5 are plotted in red stars. The values of the contour circles are only important for the inner circles to be able to compare between different values of t_0. It is not possible to read the values of the highest misfit contours, but they are not important for the localization. For station number of the stations see figure 4.4 (or 1.6) and notice that the misfit plots are somehow rotated 90 degrees compared to figure 4.4. We know that the t_0 is 12.52.00.004 and that SP2 is located in the middle of the area just above station S7. The minimum misfit corresponds well to the position of the three values of t_0. Figure 4.2

for which t_0 is closest to the real t_0 of the shot, has the largest area around the location with the lowest misfit values. The conclusion is that the misfit function can be used even if the microevents are not known. The form of the misfit function can give information on it also. Testing the five shots shows that the localization method works well. Since it was successful to locate the five shots I also concluded that the velocity model is not too bad.
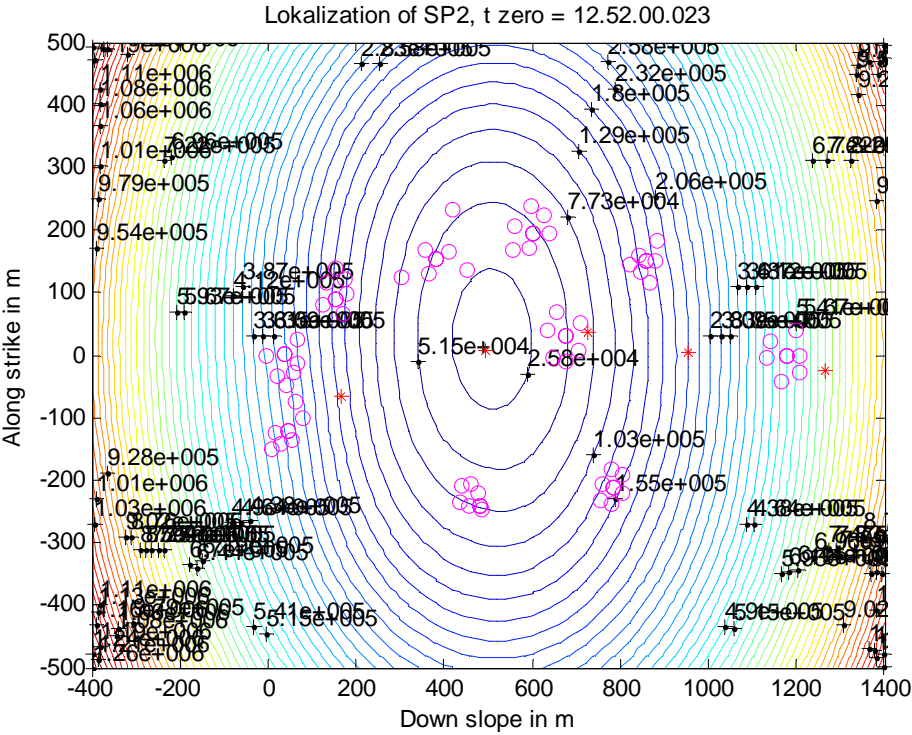
Figure 4.1: Localization of SP2, localized using t_0 = 12.52.00.023. The location of the geophones are marked with magenta circles, the locations of SP1 to SP5 are marked with red stars.
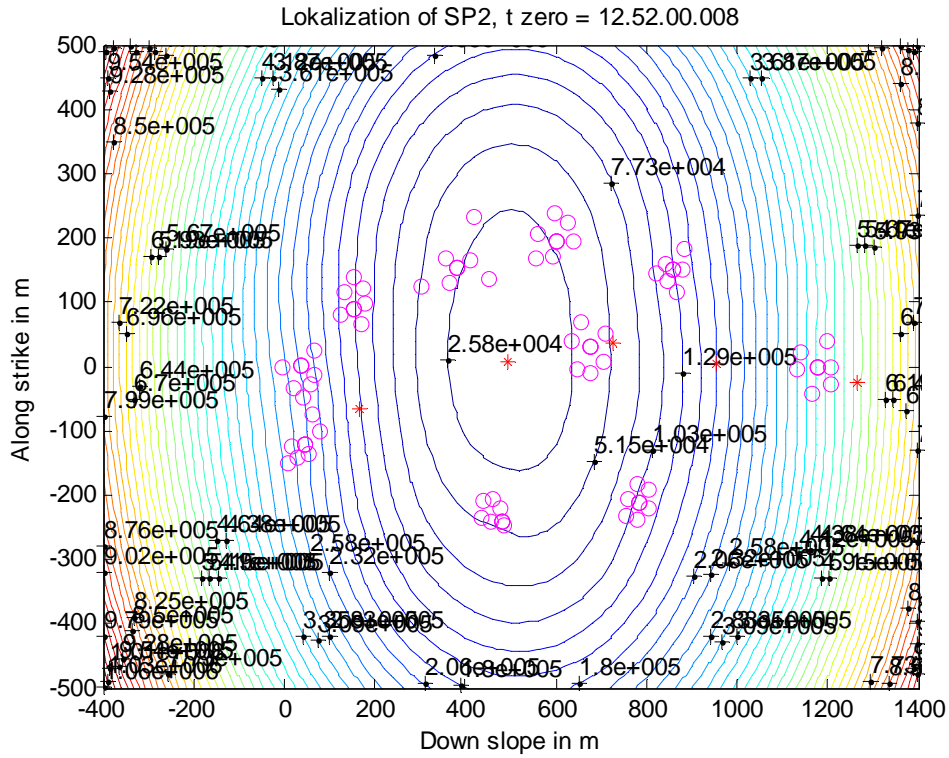
Figure 4.2: this is localization of SP2, localized wit t_0 = 12.52.00.008. The magenta circles are the location of the geophones, SP1 to SP2 are marked with red stars.
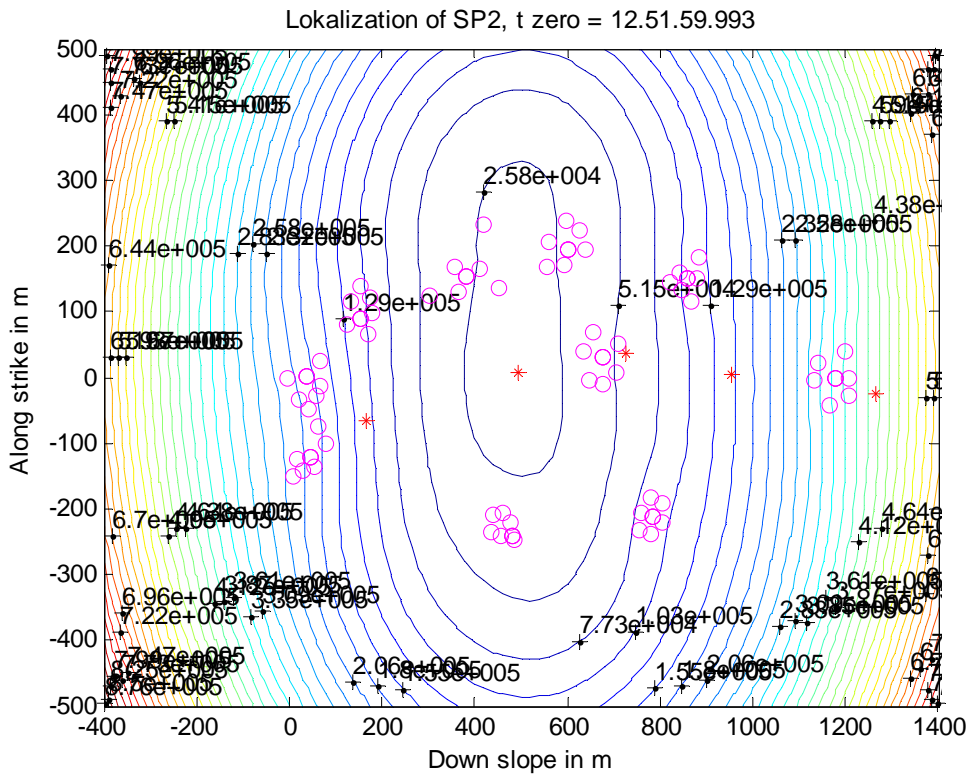
Figure 4.3: This is SP2 localized with t_0 = 12.51.59.993. The magenta circles are the location of the geophones, the red stars are the location of the shots SP1 to SP5.

4.3: Results from the localization of microevents

I have only tried to localize events nr. 2, 3, 4, 5, 7 and 8. Event nr.1 has not been tried localized because it is an earthquake with a distance of 137km to the site. Event nr. 6 has not been tried localized either, because it had no clear onset and the first arrival times could not be picked. Six micrevents have been identified and successfully localized. Figure 4.5 to 4.8 shows the results.

The misfit function of event nr 2 is plotted in figure nr 4.5. This event appears to be located at the same altitude as S10 but just outside the instable area, on the other side of the crevasse limiting the area eastward.

The misfit function of event nr 3 is plotted in figure 4.6. This is a microseismic event with origin in the lower eastern part of the instable area, about in the middle between S10 and S8.

The misfit function of event nr 4 is plotted in figure 4.7. The event appears to be located in the open fracture at the top of the area just between S1 and S2.

Event nr. 5 is also appears to located by the open fracture close the stations S1, S2 and S3.

Within a range of plus/minus 20 ms, the plots of the misfit does not vary very much with t_0 but going outside this range the plot changes. The location of the lowest misfit value does vary much with the slowness. Within a range of plus/minus 0.05 ms/m the position of minimum misfit value moves about 200 m (when the velocity changes from 4 km/s to 6.7 km/s). If the $T_{intercept}$ changes with plus/minus 40 ms the position of minimum misfit value changes 100 m in opposite directions. Within a range of plus/minus 10 ms sec the position of minimum misfit value changes less than 20 meters. Overall the success of the localization depends on having good values for $T_{intercept}$ and the slowness. This also confirms that the relation in equation 13 and 19 is a good estimation for the slope (since the localization of SP1 to SP5 was successful).
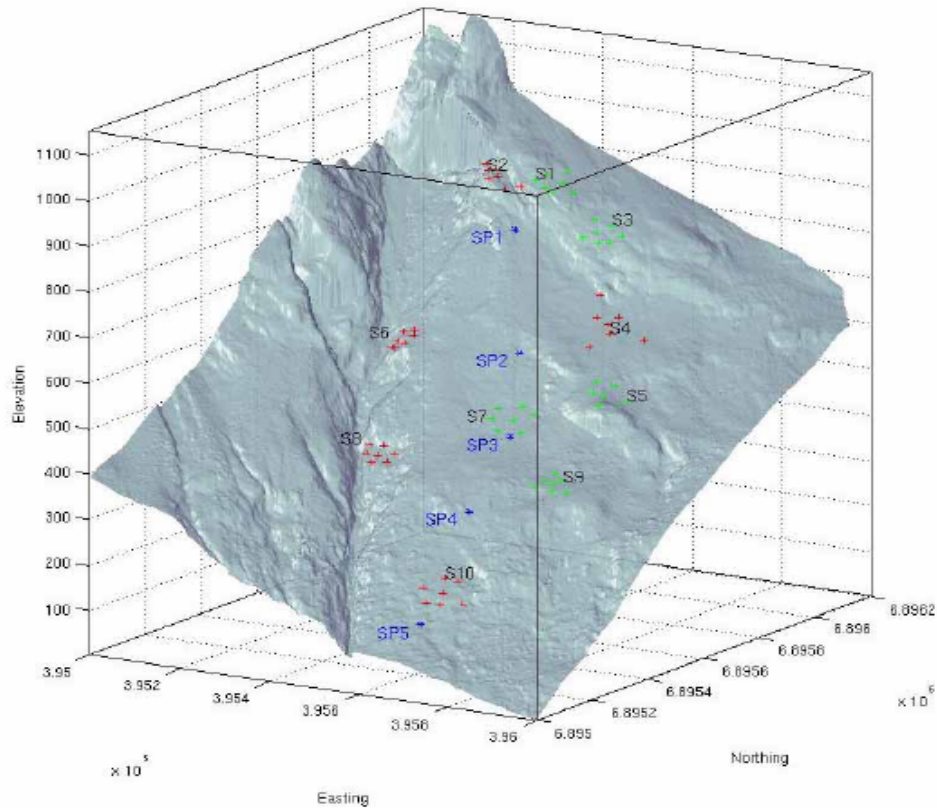
Figure 4.4: This is a topographic map of the area, with the stations (S1 to S10) and the shots of refraction seismic (SP1 to SP5) plotted. Compare this with the plots of localization to see the nr of the stations. (Frery, 2007).
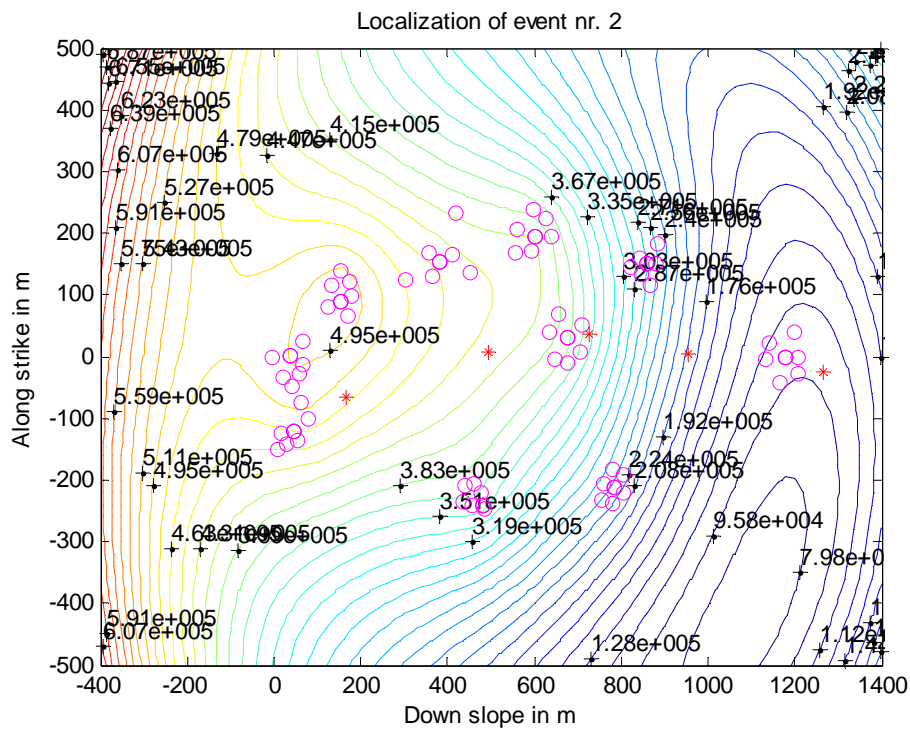
Figure 4.5: Localizing event nr. 2.
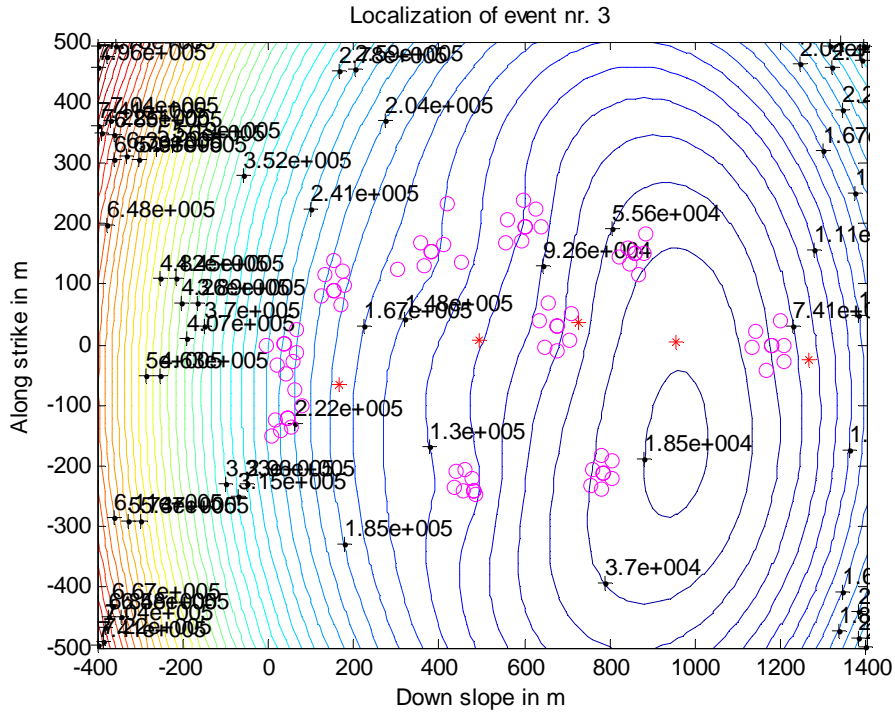
Figure 4.6: Localization of event nr 3.
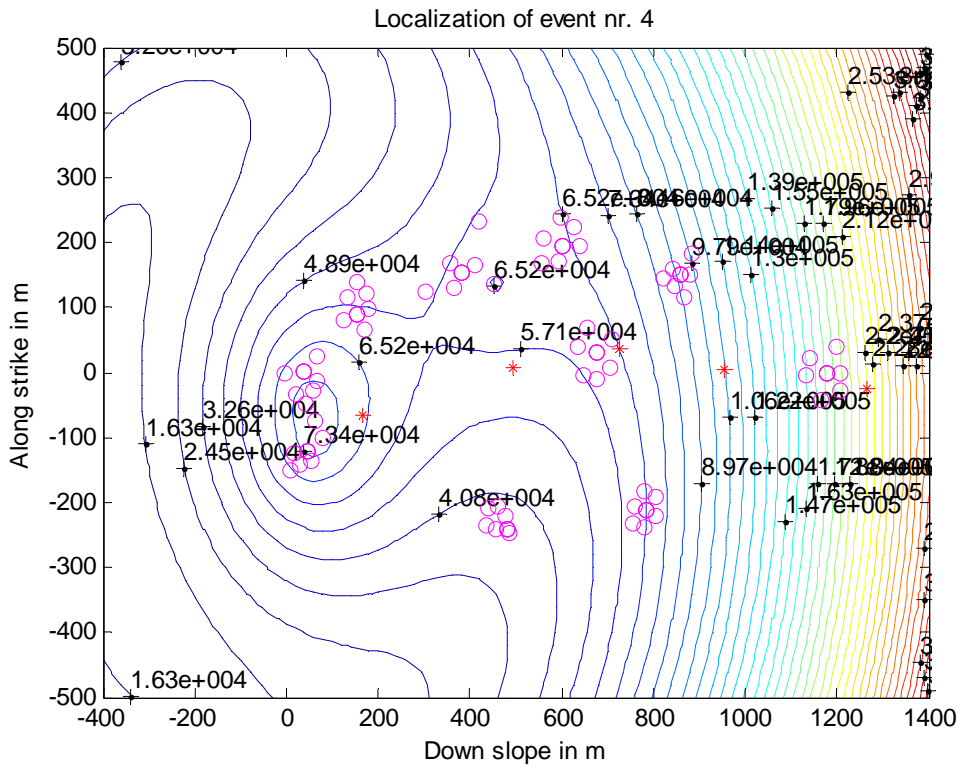
Figure 4.7: Localization of event nr 4.
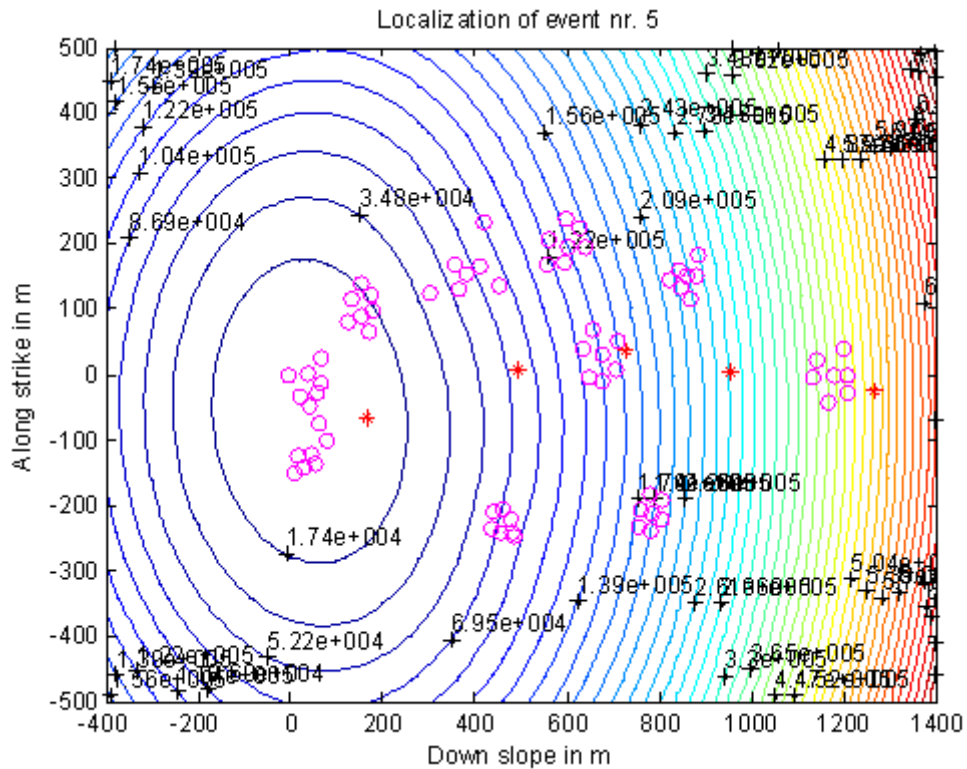
Figure 4.8: Localization of event nr 5.

Events nr 7 and 8 are the first two in a series of four events, that are recorded over a time-span of 80sec and they have a very short duration (0.8sec). The events have been recorded on stations S4, S5 and S10, which were the only ones recording at that time. The result of the localization of events nr. 7 and 8 shows highest misfit values within the area, and decreasing misfit further away. From figure 2.18 and 2.19 that the biggest difference in arrivaltimes for two components at the same station, for both event 7 and 8, is about 400 ms. The largest distance possible between two components at one station is 100 m. If a seismic wave should have traveled maximum 100 m in 400 ms it would have had a maximum velocity of 0.25 km/s. A velocity that low does not fit with the relation in equation 3.13 and 3.19. I therefore tried to change the $T_{intercept}$, t_0 and the slowness and found that the lowest value of misfit was obtained with $T_{intercept}$ equal to 0, a slowness equal to 2.39 ms/ms, and a t_0 equal to 742 ms. Figure 4.11 and 4.12 shows the localization of events 7 and 8. This result still has high misfit values around the S4 and S5, but now it implies that the source is in a SSE direction.
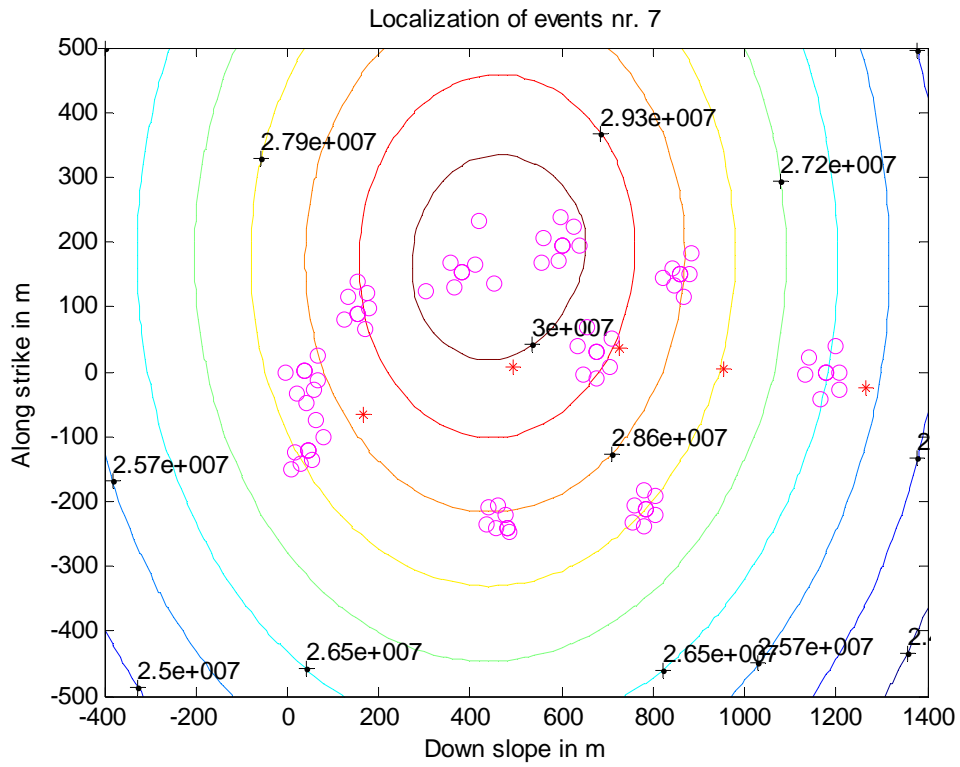
Figure 4.9: Localization of event nr. 7
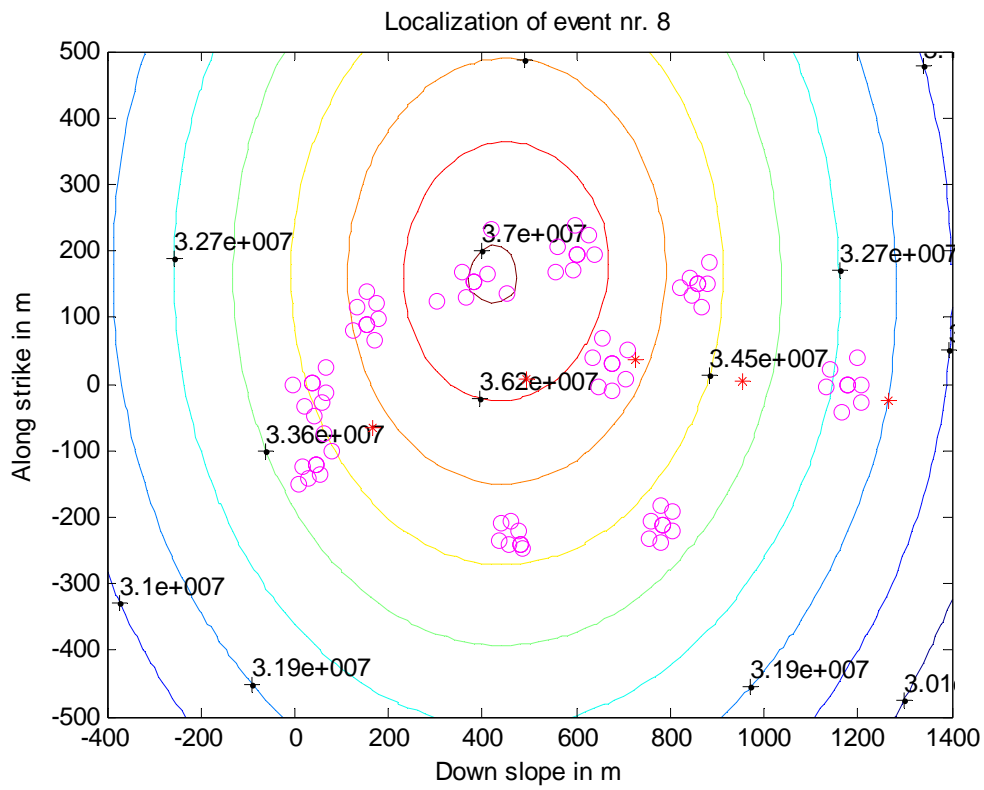
Figure 4.10: Localization of event nr. 8
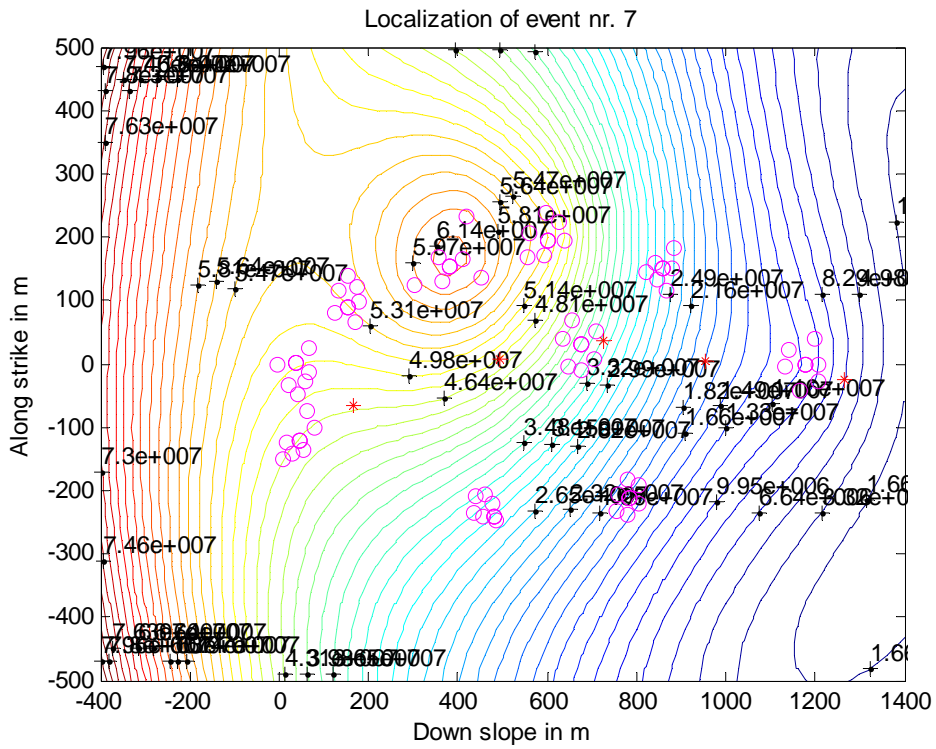
Figure 4.11: Localization of event nr 7.
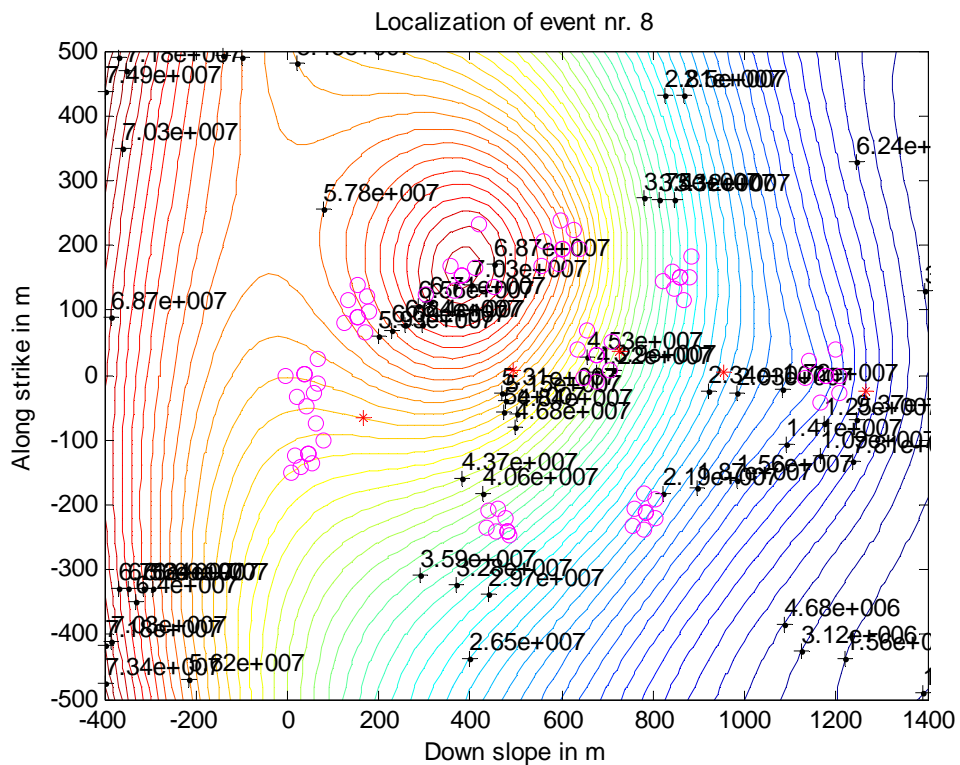
Figure 4.12: Localization of event nr 8.

5: DISCUSSION

From December 2005 to June 2006 an average of 8 to 10 events with durations under 8sec were recorded per day on the permanent seismic network (Delarue, 2006). I have found 6 events with durations under 8sec in 50 days. Taken into account that I have only analyzed half of the data, I have found about one event every fourth day. So I have found far less events than what is detected on the permanent network. Some of the reasons for this could be that, compared to the permanent seismic network, the stations in the temporary IHR network are spaced further apart from each other. And if most of the microseismic events are too weak to be registered on more than one station they will not be registered by my method. The fact that many of the stations were not operative towards the end of the recording period of the IHR system makes it even less possible for a weak event to be detected on more than one station.

It would have been interesting to look at some of the events that were recorded at all the components on one station, but not on more than one station. Because these events could be nice microseismic events perfect for localization, but not registered on more than one station for the reason explained above. Though they will be difficult to localize, one could say in which region of the slope the event comes from and thus say something about the seismic activity of the slope.

The accuracy of the localization process depends on the accuracy of the arrival time-picking and on how well the velocities have been modeled. If you have perfect velocities and perfect first arrival picks, you can do prefect localization. But for doing that you need a much more advanced localization method than I have used. One method one can use is ray tracing. With a better velocity model one could maybe have found the hypocenter of the found events nr.2, 3, 4 and 5 by using ray tracing.

The topography is not taken into account, for either the velocity modeling or the localization. So for a better velocity model it would have also been necessary to take into account the topography to be able to localize hypocenters.

There is a lot of noise in the data from field work and helicopter activity. Maybe the performance of the system would have been better if the area had been free for activities in the recording period.

6: CONCLUSION

Initially the goal of the work in this thesis was to find and locate microseismic events associated with the movement in the slope at Åknes and to be able to say something about the nature of the movement. Four events have successfully been localized, but only their epicentre, and this is not enough to say anything more about the movement than that there has been seismic activity in the slope in the localized region. The number of events registered (on more than three components at one station) for each station can say more about the seismic activity of the slope. In table 6.1 I have taken the number of events from appendix B.2, registered on each station and divided it by the nr of days each station was operational (from appendix B.1). This gives an average of events detected per day for each of the components.

Station	Events registered on more than three components	Nr. of days operational	Average nr. of events detected per day
S1	10	50	0.2
S2	30	22	1.36
S3	3	8	0.375
S4	5	43	0.116
S5	6	38	0.158
S6	16	39	0.41
S7	8	34	0.235
S8	9	45	0.2
S9	3	22	0.136

Table 6.1: The average of events detected per day for S1 to S9.

Figure 6.1 shows that S1 and some of the components of S3 is located above the open fracture limiting the instable area to the north. From table 6.1 I can conclude that the seismic activity around S2 is by far the highest. This is also where the highest movement rate is registered. S1 is located close to S2 but has low activity. This could be because S1 is located just on the stable part of the upper open fracture. S6 have also registered higher seismic activity than the other stations. It is located close to the crevasse on the west side of the area, but so is S8 with low registered activity.

Another goal was to see if overall the use of this temporary IHR system is a good approach for investigating a potential rock slide area. My conclusion is that if all the stations had been working as they should, and the performance of the system had been better than 57% of successfully recorded data, this could give much more useful information on a slide area. Also the IHR network was only recording for 6-7 weeks, and a longer recording period could give more results.
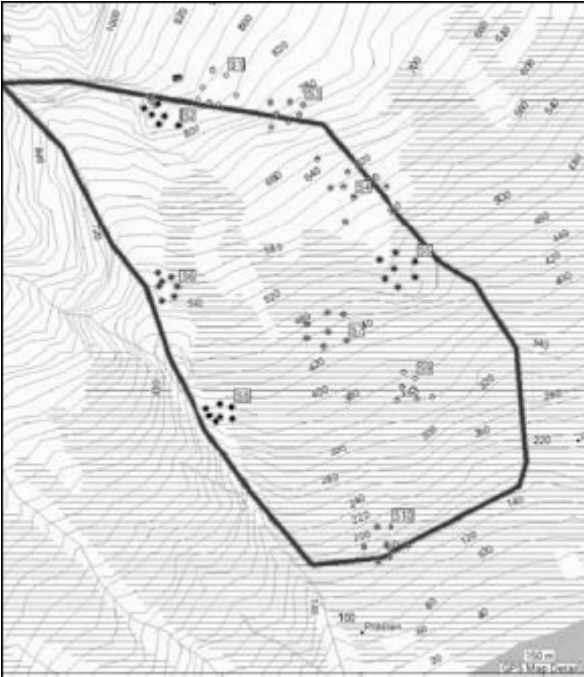
Figure 6.1: The location of the stations S1 to S10. Note that S1 and some of the components on S3 is located above the open fracture that limits the instable are to the north (Lecomte, 2006).

7: REFERENCES

Ambuter B. P. and Solomon S. C. (1974). An Event-Recording System for Monitoring Small Earthquakes. Bulletin of the Seismological Society of America. Vol. 64, No 4, pp. 1181-1188.

Blikra L. H. Anda E., Belsby S., Jogerud K., Klempe Ø. (2006). Åknes/Tafjord prosjektet, Status rapport for Arbeidrgruppe 1 (Undersøking og overvåkning)

Blikra L. H. (2006). The Åknes/Tafjord project, status and plans for 2006. Published by NGU (Norges Geologiske Undersøkelse) at Tafjord Project Workshop 20/2-21/2 2006, Trondheim.

Bonnefoy-Claudet S., Cotton F. & Bard P. (2006). The nature of noise wavefield and its applications for site effects studies, A literature review. Earth-Science Reviews 79 205-227.

Brenguier F., Coutant O., Dietrich M., Lecomte I. (2005). High resolution seismic imaging of highly heterogeneous media: An experiment on the Puy des Goules volcano, France. Geophysical Research Abstracts, vol 7, 06548, EGU Annual Meeting, Vienna.

Derron M. H., Blikra L. H., Jaboyedoff M. (2005). High resolution digital levation model analysis for landslide hazard assessment (Åkerneset, Norway). Landslide and avalanches ICFL 2005 Norway. Taylor & Francis Group, London.

Delarue C. (2006). Analysis of Microseismic Events Recorded at the Unstable Rock-Slope Site at Åknes, Norway. Diplome d'ingenieur geophysicien, EOST, University of Strasburg I, France.

Dietrich M., Lecomte I., Meric O., Roth M., Dore F., Guiguet R., De Barros L., Grasso J. –R. & Orengo Y. (2006). Åknes 2005 campaign: refraction seismics and IHR microseismic network. Åknes/Tafjord workshop 20-21.2.2006, Trondheim.

Eidsvig U. & Harbitz C. B. (2005) Innledende numeriske analyser av flodbølger som følge av mulige skred fra Åkneset. Report from NGI published at the homepages of the Åknes/Tafjord project. http://www.aknes-tafjord.no/Artikkel.aspx?AId=494&back=1&MId1=568&.

Emblemsvåg J. (2008**),** Flodbølger fra Åkneset, Kolofon Forlag AS.

Furseth A. (1985). Dommedagsfjellet: Tafjord 1934. Gyldendal Norsk Forlag. Norway.

Frery E. (2007). Seismic velocities of the unstable rock slope site at Åknes, Norway. Report from a summer job at NORSAR, not published.

Ganerød G. V., Grøneng G., Rønning J. S., Dalsegg E., Elvebakk H., Tønnesen J. F., Kveldsvik V., Eiken T., Blikra L. H., Braathen A. (2008), Geological model of the Åknes rockslide, western Norway, Engineering Geology 102 (2008) 1-18.

Høst J. (2006), Store Fjellskred i Norge, NGU Trondheim.

Lecomte I. (2006). Geophysics for investigation and analysis of large landslides. NFR BILAT # 169822/D15, NORSAR/LGIT Final Report.

Musset A. E. & Khan M. A. (2000). Looking into the Earth. Cambridge University Press. Cambridge, United Kingdom.

NGU (Norges Geologiske Undersøkelse) (2008). Berggrunnen i Norge N250. NGU, Trondheim, Norway. Downloaded from http://www.ngu.no/kart/bg250/ December, 2008.

Roth M., Dietrich M., Blikra L. H., Lecomte I. (2005). Seismic Monitoring of the Unstable Rock slope at Åknes, Norway. Extended abstract, 19th annual SAGEEP (Symposium on the Application of Geophysics to Engineering and Environmental Problems), Seattle, Washington.

Roth M. (2006). Status report 1-2006 Passive seismic monitoring at Åknes. Published at the homepages of the Åknes-Tafjord project 2006 http://aknes-tafjord.no/artikkel.aspx?MId1=578&AId=633&Back=1

Stein S. & Wysession M. (2003) An Introduction to seismology, earthquakes, and earth structure. Blackwell Publishing. Oxford, UK.

Trnkoczy A. (1998). Understanding & Setting STA/LTA Trigger Algorithm Parameters for the K2. Published at ftp://ftp.kinemetrics.com/pub/AppNotes/appnote41.PDF

Thorne M. (2004) rsac.m, http://web.utah.edu/thorne/saclab/rsac.m

Tveten E., Lutro O., Thorsnes T. (1998). Berggrunnskart Ålesund 1:250 000, (Ålesund, western Norway). NGU Trondheim (bedrock map).

APPENDIX A: Matlab PROGRAMS

Appendix A.1: rsac.m (Thorne M. 2004).

```
%RSAC    Read SAC binary files.
%    RSAC('sacfile') reads in a SAC (seismic analysis code) binary
%    format file into a 3-column vector.
%    Column 1 contains time values.
%    Column 2 contains amplitude values.
%    Column 3 contains all SAC header information.
%    Default byte order is big-endian.  M-file can be set to default
%    little-endian byte order.
%
%    usage:  output = rsac('sacfile')
%
%    Examples:
%
%    KATH = rsac('KATH.R');
%    plot(KATH(:,1),KATH(:,2))
%
%    [SQRL, AAK] = rsac('SQRL.R','AAK.R');
%
%    by Michael Thorne (4/2004)    mthorne@asu.edu

function [varargout] = rsac(varargin);

for nrecs = 1:nargin

  sacfile = varargin{nrecs};

%-------------------------------------------------------------------------
-
%    Default byte-order
%    endian  = 'big-endian' byte order (e.g., UNIX)
%            = 'little-endian' byte order (e.g., LINUX)

endian = 'little-endian';

if strcmp(endian,'big-endian')
  fid = fopen(sacfile,'r','ieee-be');
elseif strcmp(endian,'little-endian')
  fid = fopen(sacfile,'r','ieee-le');
end

% read in single precision real header variables:
%-------------------------------------------------------------------------
-
for i=1:70
  h(i) = fread(fid,1,'single');
end

% read in single precision integer header variables:
```

```
%------------------------------------------------------------------------
-
for i=71:105
  h(i) = fread(fid,1,'int32');
end


% Check header version = 6 and issue warning
%------------------------------------------------------------------------
-
% If the header version is not NVHDR == 6 then the sacfile is likely of the
% opposite byte order.  This will give h(77) some ridiculously large
% number.  NVHDR can also be 4 or 5.  In this case it is an old SAC file
% and rsac cannot read this file in.  To correct, read the SAC file into
% the newest verson of SAC and w over.
%
if (h(77) == 4 | h(77) == 5)
    message = strcat('NVHDR = 4 or 5. File: "',sacfile,'" may be from an
old version of SAC.');
    error(message)
elseif h(77) ~= 6
    message = strcat('Current rsac byte order: "',endian,'". File:
"',sacfile,'" may be of opposite byte-order.');
    error(message)
end

% read in logical header variables
%------------------------------------------------------------------------
-
for i=106:110
  h(i) = fread(fid,1,'int32');
end

% read in character header variables
%------------------------------------------------------------------------
-
for i=111:302
  h(i) = (fread(fid,1,'char'))';
end

% read in amplitudes
%------------------------------------------------------------------------
-

YARRAY     = fread(fid,'single');

if h(106) == 1
  XARRAY = (linspace(h(6),h(7),h(80)))';
else
  error('LEVEN must = 1; SAC file not evenly spaced')
end

% add header signature for testing files for SAC format
%------------------------------------------------------------------------
-
h(303) = 77;
h(304) = 73;
h(305) = 75;
```

```
h(306) = 69;

% arrange output files
%-----------------------------------------------------------------------------
-
OUTPUT(:,1) = XARRAY;
OUTPUT(:,2) = YARRAY;
OUTPUT(1:306,3) = h(1:306)';

%pad xarray and yarray with NaN if smaller than header field
if h(80) < 306
  OUTPUT((h(80)+1):306,1) = NaN;
  OUTPUT((h(80)+1):306,2) = NaN;
end

fclose(fid);

varargout{nrecs} = OUTPUT;

end
end
```

Appendix A.2: findevents.m

```
function [A] = findevents(sacfil,argin)


a = str2num(argin(32));      %This is done to make the header information

b = str2num(argin(34));      %into an integer to avoid printing problems

c = str2num(argin(35));      %later.

d = str2num(argin(37));

e = str2num(argin(38));

%f = str2num(argin(15));      %scipping the minutes and seconds to make the

%g = str2num(argin(16));      %number have fewer digits.

%h = str2num(argin(18));

%i = str2num(argin(19));

j = str2num(argin(47));

k = str2num(argin(53));


l = [a b c d e j k];         %make a matrix with the digits from the header.

header1 = sprintf('%1d',l);  %making one string from the elements of l.

header = str2num(header1);   %convertng the string into an integer.


nr = size(sacfil);           %The size of the sacfile gives the nr of

N = nr(1,1);                 %samplingpoints N.
```

```matlab
K = [1:N];                     %gives the first colomb the nr of
-                              %samplingpoint.


sacfil(:,1) = K;


%lta = std(sacfil(:,2));       %to keep the lta the same value.(doesn't work)


event = [0 0 0];
%event = zeros(10,3);          %Define a matrix that holds the registered
j = 0;                         %events if any. j counts.


stalta = zeros(1,N);           %Define vektor that holds the values of
                               %STA/LTA.
%n1 = 120000;                  %Long term average in nr of samplingpoints.
%n2 = 32000;                   %Short term average.
%begin = 1.5;                  %Treshold for registrering an event.
%finish = 1.5;                 %Treshold for stop registrering.


n1 = 500;
n2 = 50;
begin = 3;
finish = 3;


regevent = 0;                  %to test if registration should be done.


for i = 1:10:N-n1
    y = i+n1-n2;
    %if regevent == 0                          %When an event is registered
    %    lta = std(sacfil(i:x,2));             %the LTA will keep it's value
    %end                                       %untill the stalta reach stop.
                                               %(this takes to long)
    lta = std(sacfil(i:i+n1,2));
    sta = std(sacfil(y:i+n1,2));
    stalta(i) = sta/lta;


    if (stalta(i) >= begin) & (regevent == 0)
            j = j+1;
```

```
            event(j,1) = i;
            regevent = 1;
    end


    if (stalta(i) <= finish) & (regevent == 1)
            event(j,2) = i;
            event(j,3) = header;
            regevent = 0;
    end


    %if mod(i,1000) == 0    %loop to follow the calculation on screen,
    %    i                  %prints out avery 100 i.
    %end
end


R = max(sacfil(:,2));
S = min(sacfil(:,2));
figure
subplot(2,1,1); plot(stalta); title('STA/LTA')
xlabel('samplingpoint 900000 pr hour'); ylabel('STA/LTA')
title(argin)
subplot(2,1,2); plot(sacfil(:,1),sacfil(:,2)); title('Seismogram')
ylim([S R])
xlabel('sampling (250 pr sec)'); ylabel('amplitude')


%plot(sacfil(:,1),sacfil(:,2)); title('Seismogram')
%ylim([S R])
%xlabel('sampling (250 pr sec)'); ylabel('amplitude')


A = event;
```

Appendix A.3: makefilenames.m

```
fid = fopen('/mn/sokrates/geo-master-u1/mariahn/mastern/281-
290filelist.allstations','r');


tline = fgetl(fid);
[x] = strtok(tline);
```

```
filenames = x;
eof = 0;
while (eof == 0)
  tline = fgetl(fid);
  if(tline == -1)
    eof = -1;
    break;
  end
  [x] = strtok(tline);
  filenames = [filenames;x];
end
```

Appendix A.4: runfiles.m

```
a = size(filenames);
n = a(1,1);

for i=1:n
    fid = fopen('found9','a');
    M = rsac(filenames(i,:));
    event = find2(M,filenames(i,:));
    a = size(event);
    b = a(1,1);

    if event(1,1)>0
        fprintf(fid,'%s\n',filenames(i,:));

        for j=1:b
        fprintf(fid,'%d,%d,%d\n',event(j,:));
        end
    end

    fclose(fid);

end
```

Appendix A.5: findvelSPall.m

```
function [A] = findvelSPall

t1 = 113100003.94;   %Trigger times plus a delay of 3.94 msec.
t2 = 125200003.94;
t3 = 134800003.94;
t4 = 080900003.94;
t5 = 091700003.94;

load artime        %first coloumb contains the nr of the stations, the
load distSPall     %following coulombs sontains the arival times and the
                   %distances to the five shotpoints.
j = 1;
k = 1;
l = 1;
m = 1;
n = 1;

for i = 1:90
    if artime(i,2) > 0
        v1(j,2) = distSPall(i,2)/(artime(i,2)-t1);
        v1(j,1) = distSPall(i,1);
        v1(j,3) = distSPall(i,2);
        v1(j,4) = artime(i,2)-t1;
        j = j+1;
    end
end


for i = 1:90
    if artime(i,3) > 0
        v2(k,2) = distSPall(i,3)/(artime(i,3)-t2);
        v2(k,1) = distSPall(i,1);
        v2(k,3) = distSPall(i,3);
        v2(k,4) = artime(i,3)-t2;
        k = k+1;
    end
end


for i = 1:90
    if artime(i,4) > 0
        v3(l,2) = distSPall(i,4)/(artime(i,4)-t3);
        v3(l,1) = distSPall(i,1);
        v3(l,3) = distSPall(i,4);
        v3(l,4) = artime(i,4)-t3;
        l = l+1;
    end
end


for i = 1:90
    if artime(i,5) > 0
        v4(m,2) = distSPall(i,5)/(artime(i,5)-t4);
        v4(m,1) = distSPall(i,1);
        v4(m,3) = distSPall(i,5);
        v4(m,4) = artime(i,5)-t4;
        m = m+1;
```

```
        end
end

for i = 1:90
    if artime(i,6) > 0
        v5(n,2) = distSPall(i,6)/(artime(i,6)-t5);
        v5(n,1) = distSPall(i,1);
        v5(n,3) = distSPall(i,6);
        v5(n,4) = artime(i,6)-t5;
        n = n+1;
    end
end
%The content of the velocity matrixes v1, v2, v3, v4 and v5:
%coulomb 1: the komponents number. (with a number one in front)
%coulomb 2: the calculated velocity.
%coulomb 3: the direct distance from the shotpoint.
%coulomb 4: the traveltimes.
av1 = sum(v1(:,2))/j;
av2 = sum(v2(:,2))/k;
av3 = sum(v3(:,2))/l;
av4 = sum(v4(:,2))/m;
av5 = sum(v5(:,2))/n;

B = [v1;v2;v3;v4;v5];
avAll = sum(B(:,2))/(j+k+l+m+n)
%Want to plot the traveltimes vs increasing distance from the shot point to
%find a velocity gradient with depth. The longer the waves have traveled,
%the deeper the waves have traveled.

scatter(B(:,3),B(:,4))
xlabel('distance from SP')
ylabel('traveltime ms')
figure
scatter(v1(:,3),v1(:,4),'r')
xlabel('distance from SP')
ylabel('traveltime ms')
hold on
scatter(v2(:,3),v2(:,4),'b')
scatter(v3(:,3),v3(:,4),'g')
scatter(v4(:,3),v4(:,4),'y')
scatter(v5(:,3),v5(:,4),'m')
legend('v1','v2','v3','v4','v5')

A = [av1;av2;av3;av4;av5];
```

Appendix A.6: lokalisering.m

```
% map the misfit to localize microevents in Aaknes

format COMPACT
format SHORT G

% load the positions of the stations in East-North-altitude
load positions;
pos=positions;
```

```
clear positions;
[nstat,ncoord]=size(pos);

% calculate positions relative to component S1-3 (northernmost station,
% almost at the top)
iref=3;
for i=1:nstat;
   posrel(i,:)=pos(i,:)-pos(iref,:);
end;
posrel;
meanelv=mean(posrel(:,3))
stdelv=std(posrel(:,3))

% rotate the coordinate system to get horizontal coordinates in max-dip -
% along topo system and turn to get positive downwards

h=4.;                    % reference moved 4 meters below point 3 to get best
                         % fit of ref. plane
alpha=72.;               % azimuth of along-topo lines, in degrees
dip=35.9;                % dip of plane

rot1=[cosd(alpha), -sind(alpha),0.; sind(alpha),cosd(alpha),0.; 0.,0.,1.];
rot2=[cosd(dip), 0., -sind(dip); 0.,1.,0.; sind(dip),0.,cosd(dip)];
for i=1:nstat;
  temp=posrel(i,:)';
  temp(3)=temp(3)+h;
  temp=rot1*temp;
  temp=rot2*temp;
  temp(3)=-temp(3);
  posrot(i,:)=temp';
end;

% check the values of the average and standard deviations of new vertical
% coordinate to verify the plane has been chosen properly
posrot;
meanelv=mean(posrot(:,3))
stdelv=std(posrot(:,3))
%-------------------------------------------------------------------------
%locations of the five shots
locSP =
[395362,6895946,772;395512,6895725,572;395598,6895552,440;395629,6895355,32
4;395679,6895103,142];
for i=1:5
    locrel(i,:)=locSP(i,:)-pos(iref,:);
end
for i=1:5
    temploc = locrel(i,:)';
    temploc=rot1*temploc;
    temploc=rot2*temploc;
    locSProt(i,:)=temploc;
end
%-------------------------------------------------------------------------


% load the arrival times of the microevents
load eventArTimes;
[nstat2,nevent]=size(eventArTimes);
if (nstat2~=nstat)
```

```
    disp ('discrepancy in number of stations in the two files')
end


% dimensions of the search
timeinterval=120;                   % time interval before minimum read time,
                                    % for which the search will be done in ms
xmin=-400;                          % up and downdip coordinate
xmax=1400;
ymin=-500;                          % strike coordinate
ymax=500;
% increments in the search
dt=120;
dx=20.;
dy=20;
%initialize arrays related to the search
xnodes=xmin:dx:xmax;
ynodes=ymin:dy:ymax;
tnodes=-120:dt:timeinterval;        %note this has to be used backwards in
time
nx=length(xnodes);
ny=length(ynodes);
nt=length(tnodes);
%-----------------------------------------------------------------------
%tnode for event nr 2 is 88
%tnode for event nr 3 is 38
%tnode for event nr 4 is 103
%tnode for event nr 5 is 29
%tnode for event nr 6 is
%tnode for event nr 7 is
%tnode for event nr 8 is
%-----------------------------------------------------------------------

% initialize the parameters of the theoretical traveltime curve
t0 = 44;                         % 44 ms
slowness=0.19;                   % 0,19 ms/m

%for i=2:nevent;      % start on 2 because first column is not an event
for i=7:7;

   for j=1:nstat2;
      if (eventArTimes(j,i)~=0);
        tt(j)=eventArTimes(j,i); % fill inn a vector
      else
        tt(j)=NaN;
      end;                             %put all the zeroes as NaN
   end
   tmin= min(tt);                      % tmin used as reference time from then on

   for ix=1:nx;
      for iy=1:ny;
         for it=1:nt;
         misfit(ix,iy,it)=0;
           for is=1:nstat2;
              if (~isnan(tt(is)));
                dist= sqrt( (xnodes(ix)-posrot(is,1))^2 + (ynodes(iy)-
posrot(is,2))^2 );
                traveltheo = t0 + slowness*dist;   % theoretical traveltime
                travelmeas = tt(is)-tmin+tnodes(it);
```
74

```
                        % measured traveltime if source was tnodes(it) before tmin
                        dmisfit = (travelmeas-traveltheo)^2;
                        misfit(ix,iy,it)= misfit(ix,iy,it)+dmisfit ;
                    end;
                end;
            end
        end
    end

    m1=min(misfit,[],1);
    m2=min(m1,[],2)

    m1=max(misfit);
    m2=max(m1);
    m3=max(m2);
    lines=50;
    colorvec=linspace(0,m3,50);

    for it=1:nt;
        figure
        slice=misfit(:,:,it);
        contour(xnodes,ynodes,slice',colorvec)
        colorbar
        A = contour(xnodes,ynodes,slice',colorvec);
        clabel(A)
        xlabel('Down slope in m')
        ylabel('Along strike in m')
        hold on
        scatter(posrot(:,1),posrot(:,2),'m')
        scatter(locSProt(:,1),locSProt(:,2),'r','*')
    end

end;
```

APPENDIX B: TABLES

Appendix B.1: Table of files run in findevents.m. The day and station marked with an x is successfully run. The days and stations marked with – does not exist in the data.

dag/stasjon	1	2	3	4	5	6	7	8	9	10	filelist name:	event is stored in:
240-28/8	x	x	x	x	x	x	x	x	-	-	240-243filelist.allstations	found2
241-29/8	x	x	x	x	x	x	x	x	-	-	240-243filelist.allstations	found2
242-30/8	x	x	x	x	x	x	x	x	x	-	240-243filelist.allstations	found2
243-31/8	x	x	x	x	x	x	x	x	x	-	240-243filelist.allstations	found2
1/9 244	x	x	[0-6]	x	x	x	x	x	x	L	244-247filelist-allstations	found3
2/9 245	x	x	-	x	x	x	x	x	x	L	244-247filelist-allstations	found3
3/9 246	x	x	-	x	x	x	x	x	x	L	244-247filelist-allstations	found3
4/9 247	x	x	-	x	x	x	x	x	x	L	244-247filelist-allstations	found3
5/9 248	x	x	-	x	x	x	x	x	x	L	248-251filelist.allstations	found4
6/9 249	x	[0-6]	-	x	x	x	x	x	x	L	248-251filelist.allstations	found4
7/9 250	x	-	-	x	x	x	x	x	x	[0-6]	248-251filelist.allstations	found4
8/9 251	x	-	-	x	x	x	x	x	x	-	248-251filelist.allstations	found4
9/9 252	x	-	-	x	x	x	x	x	x	-	252-255filelist.allstations	found5
10/9 253	x	-	-	x	x	x	x	x	x	-	252-255filelist.allstations	found5
11/9 254	x	-	-	x	-	x	x	x	x	-	252-255filelist.allstations	found5
12/9 255	x	x	-	x	-	x	x	x	[0-6]	-	252-255filelist.allstations	found5
13/9 256	x	x	-	x	-	x	x	x	-	-	256-260filelist.allstations	found6
14/9 257	x	x	-	x	-	x	x	x	-	-	256-260filelist.allstations	found6
15/9 258	x	x	-	x	-	x	x	x	-	-	256-260filelist.allstations	found6
16/9 259	x	x	-	x	-	x	x	x	-	-	256-260filelist.allstations	found6
17/9 260	x	x	-	x	-	x	x	[0-6]	-	-	256-260filelist.allstations	found6
18/9 261	x	-	-	x	-	x	x	-	-	-	261-270filelist.allstations	found7

Date	1	2	3	4	5	6	7	8	9	L	filelist	found
19/9 262	x	-	-	x	-	x	x	-	-	-	261-270filelist.allstations	found7
20/9 263	x	-	-	x	-	x	x	-	-	-	261-270filelist.allstations	found7
21/9 264	x	-	-	x	-	x	x	x	-	-	261-270filelist.allstations	found7
22/9 265	x	-	-	x	[20-23]	x	x	x	-	-	261-270filelist.allstations	found7
23/9 266	x	-	-	-	x	x	x	x	-	-	261-270filelist.allstations	found7
24/9 267	x	-	-	-	x	x	x	x	-	-	261-270filelist.allstations	found7
25/9 268	x	-	-	-	x	x	x	x	-	-	261-270filelist.allstations	found7
26/9 269	x	-	-	-	x	x	x	x	-	-	261-270filelist.allstations	found7
27/9 270	x	-	-	-	x	x	x	x	-	-	261-270filelist.allstations	found7
28/9 271	x	-	-	-	x	x	-	x	-	-	271-280filelist.allstations	found8
29/9 272	x	-	-	-	x	x	-	-	-	-	271-280filelist.allstations	found8
30/9 273	x	[0-6]	-	[20-23]	x	[0-6]	-	[20-23]	-	[20-23]	271-280filelist.allstations	found8
1/10 274	x	-	-	x	x	-	-	x	-	L	271-280filelist.allstations	found8
2/10 275	x	-	-	x	x	-	-	x	-	L	271-280filelist.allstations	found8
3/10 276	x	-	-	x	x	-	-	x	-	-	271-280filelist.allstations	found8
4/10 277	x	-	-	x	x	-	-	x	-	-	271-280filelist.allstations	found8
5/10 278	x	-	-	x	x	-	-	x	-	-	271-280filelist.allstations	found8
6/10 279	x	-	-	x	[0-6]	-	-	x	-	-	271-280filelist.allstations	found8
7/10 280	x	-	-	x	[20-23]	-	-	x	-	-	271-280filelist.allstations	found8
8/10 281	x	-	-	x	x	-	-	x	-	-	281-290filelist.allstations	found9
9/10 282	x	-	-	x	[0-6]	-	-	[0-6]	-	-	281-290filelist.allstations	found9
10/10 283	x	-	-	x	-	-	-	-	-	-	281-290filelist.allstations	found9
11/10 284	x	[20-23]	-	x	[20-23]	[20-23]	-	[20-23]	[20-23]	[20-23]	281-290filelist.allstations	found9
12/10 285	x	x	-	x	x	[0-6]	-	x	x	L	281-290filelist.allstations	found9
13/10 286	x	x	-	x	x	-	-	x	x	L	281-290filelist.allstations	found9
14/10 287	x	[0-6]	-	x	x	-	-	x	x	L	281-290filelist.allstations	found9
15/10 288	x	-	[20-23]	x	x	-	-	[0-6]	[20-23]	L	281-290filelist.allstations	found9
16/10 289	x	[20-23]	x	x	x	[20-23]	[20-23]	-	x	L	281-290filelist.allstations	found9
17/10 290	x	x	x	x	x	x	x	-	x	L	281-290filelist.allstations	found9

Appendix B.2: This table shows all the events that has been registered on more than four components. The events that have been registered on more than two stations are marked with gray and given a number in the last column.

Station	Day	hour	start time	end time	komponents	from found file	Eventnr:
S2	240	22	773161	773241	0,1,2,4,5,7	found2	1
S3	240	22	773271	773341	0,2,3,4,5	found2	1
S4	240	22	773321	773411	0,1,3,4,5,6,7,8	found2	1
S5	240	22	773141	773191	0,1,2,3,5	found2	1
S6	240	22	773301	773351	1,2,3,4,5,6,7,8	found2	1
S6	240	23	321741	321811	1,2,3,4,5,6,7,8	found2	
S7	240	22	773231	773301	3,4,6,7,8	found2	
S2	241	2	79031	79091	1,4,5,6,7	found2	
S6	241	21	187791	187831	0,2,3,6,8	found2	
S5	242	21	112391	112451	0,1,2,5	found2	2
S6	242	21	112371	112441	1,2,3,4,5,6,7,8	found2	2
S7	242	21	112461	112531	0,2,3,4,5,6,7,8	found2	2
S8	242	21	112301	112371	1,2,3,4,5,6,7,8	found2	2
S9	242	21	112401	112471	1,2,3,4,5,6	found2	2
S2	243	0	516711	516821	1,2,4,5,6,7	found2	
S7	243	6	421401	421461	0,2,3,4,7,8	found2	
S7	243	6	722391	722491	0,3,4,5,6,7,8	found2	
S3	244	3	292761	292821	0,1,2,3,4,5	found3	
S2	245	0	395941	395991	1,2,4,5,6,7,8	found3	
S6	245	6	346461	346601	1,2,3,4,6,7,8	found3	
S7	245	20	238261	238201	1,2,3,4,7	found3	
S5	247	21	253321	253401	0,1,2,3,5,6	found3	3
S6	247	21	253281	253341	1,2,3,4,5,6,8	found3	3
S7	247	21	253491	253571	0,2,3,4,5,6,7,8	found3	3
S8	247	21	253391	253461	0,1,3,4,5,6,7,8	found3	3
S9	247	21	252401	253471	1,2,4,6	found3	3
S1	248	2	378931	378981	2,5,7,8	found4	4
S1	248	5	570161	570211	0,1,2,3,5,6	found4	5
S2	248	1	709681	709791	all !!	found4	
S2	248	2	378851	378951	all !!	found4	4
S2	248	4	513751	513831	1,3,4,6,7,8	found4	
S2	248	5	570121	570221	all !!	found4	5

S2	248	20	566161	566231	4,5,6,7,8	found4	
S4	248	5	570061	570121	1,4,5,6,8	found4	5
S8	248	22	496911	496971	0,1,4,8	found4	
S2	249	4	628161	628231	0,1,2,5,6,7,8	found4	
S2	249	6	720661	720721	1,4,6,7	found4	
S6	252	2	810471	810531	1,3,5,6,7,8	found5	
S1	253	4	247171	247221	1,6,7,8	found5	
S1	253	6	540581	540631	0,1,3,5,6,7,8	found5	6
S6	253	3	415771	415851	3,5,6,7,8	found5	
S6	253	6	540601	540681	1,2,3,4,5,6,7,8	found5	6
S6	253	20	790951	790961	1,3,4,5,6,7,8	found5	
S8	253	5	222501	222551	2,4,5,8	found5	
S8	254	21	732941	732991	0,1,4,5,7,8	found5	
S1	255	4	17551	17601	0,1,3,6,7,8	found5	
S1	255	4	561671	561721	0,6,7,8	found5	
S2	255	6	34101	34141	0,1,2,3,4	found5	
S2	255	20	51141	51221	0,1,2,4,5,6,7,8	found5	
S2	255	22	811541	811601	1,5,6,8	found5	
S6	256	1	501181	501251	3,5,6,7,8	found6	
S2	257	20	669251	669311	3,6,7,8	found6	
S2	257	21	518501	518551	0,2,6,7	found6	
S2	257	22	680001	680071	0,1,2,7,8	found6	
S1	258	5	749851	749921	0,2,3,5,6	found6	
S2	258	6	659221	659351	all !!	found6	
S6	258	6	42501	42551	1,2,3,5,6,7,8	found6	
S6	258	6	308361	208681	5,6,7,8	found6	
S2	259	0	593961	594081	0,1,2,6,7,8	found6	
S2	259	1	766861	766921	0,2,6,7,8	found6	
S2	259	20	82291	82311	0,3,4,6,7	found6	
S2	259	22	626811	626861	2,3,6,7,8	found6	
S2	259	23	386861	386911	1,2,3,4,5,6,7,8	found6	
S2	260	1	773221	773291	all !!	found6	
S2	260	4	2181	2221	1,2,3,4,5,6,7,8	found6	
S2	260	5	245721	245751	4,5,6,7,8	found6	
S6	260	2	381001	381071	1,3,5,6,7,8	found6	
S6	260	5	110181	110221	1,3,5,6,7,8	found6	
S6	261	20	345251	345261	3,4,5,6,7,8	found7	
S7	262	4	852871	852901	2,6,7,8	found7	
S1	267	20	212271	212321	0,1,6,7,8	found7	

S6	267	4	806561	806611	3,5,6,8	found7	
S8	267	0	571531	571581	0,6,7,8	found7	
S8	270	1	43921	43991	1,4,6,7,8	found7	
S8	270	6	453191	453201	1,4,5,6,7	found7	
S6	271	3	67971	67981	1,6,7,8	found8	
S1	272	1	357501	357551	0,1,6,7,8	found8	
S8	285	20	601001	601031	2,6,7,8	found9	
S1	287	3	64191	64241	0,1,3,5,6,7,8	found9	
S2	287	3	64191	64241	all !!	found9	
S4	288	6	678061	678141	2,3,4,5,6,7,8	found9	7
S4	288	6	684861	684901	2,3,4,5,6,7,8	found9	8
S5	288	6	677811	677851	0,4,6,7,8	found9	7
S5	288	6	684621	684671	0,4,6,7,8	found9	8
S5	288	6	893731	893771	0,1,3,4,5,6,7,8	found9	
S2	289	20	668191	668291	2,5,6,7	found9	
S3	289	4	590091	590141	2,3,4,5	found9	
S5	289	1	367191	367231	3,6,7,8	found9	
S2	290	4	411481	411521	0,1,6,7,8	found9	
S2	290	20	145771	145801	2,3,4,5,6,7,8	found9	
S4	290	6	603141	603171	1,2,3,5,7	found9	
S7	290	2	595461	595471	1,2,6,7	found9	
S9	290	5	554031	554081	4,5,6,7,8	found9	

Appendix B.3: Positions and times for the five shots from the refraction seismic survey (Frery 2007).

Shot	Northing (m)	Easting (m)	Elevation (m)	Day	Trigger time (UTC)
SP1	6895946	395362	772	16. Oct 2005	11:31
SP2	6895725	395512	572	16. Oct 2005	12:52
SP3	6895552	395598	440	16. Oct 2005	13:48
SP4	6895355	395629	324	17. Oct 2005	08:09
SP5	6895103	395679	142	17. Oct 2005	09:17

Appendix B.4: Position of all the components. The 3-component geophones are marked with bold letters. Here the components are not labeled the same way as in the data, the two first columns of appendix B.5 shows the correspondence.

Geophone	Easting (m)	Northing (m)	Elevation (m)	Sensor	Comments
S1-1	395351	6896037	860	1c	
S1-2	395359	6896061	868	1c	
S1-3	395383	6896096	870	1c	
S1-4	395396	6896060	853	3c	
S1-5	395426	6896045	837	1c	
S1-6	395392	6896030	841	1c	Along main fracture
S1-7	395375	6896032	847	1c	Along main fracture
S2-1	395331	6896012	850	1c	Under top cliff, water drops
S2-2	395311	6895989	843	1c	Stone-covered ridge
S2-3	395273	6895994	860	1c	Edge of bottom cliff
S2-4	395260	6896012	873	1c	Stone-covered ridge
S2-5	395247	6896026	882	1c	"Razor blade"
S2-6	395272	6896032	872	1c	Central graben
S2-7	395284	6896008	863	3c	Stone-covered ridge
S3-1	395524	6896034	783	1c	
S3-2	395553	6896023	769	1c	
S3-3	395539	6896004	757	1c	Close to a small stream
S3-4	395505	6896006	773	3c	
S3-5	395489	6896026	794	1c	
S3-6	395519	6895992	756	1c	
S3-7	395488	6895987	764	1c	
S4-1	395571	6895917	665	1c	Station S4 installed in the
S4-2	395594	6895868	630	1c	middle of a grassy slope
S4-3	395628	6895890	630	1c	(talus)
S4-4	395637	6895845	606	1c	Below main fracture
S4-5	395622	6895797	587	1c	
S4-6	395703	6895863	596	1c	
S4-7	395621	6895864	619	3c	
S5-1	395756	6895717	501	1c	Station S5 deployed
S5-2	395717	6895694	514	3c	around landing platform P4
S5-3	395754	6895682	497	1c	
S5-4	395732	6895655	505	1c	
S5-5	395682	6895722	535	1c	
S5-6	395695	6895692	519	1c	
S5-7	395716	6895736	527	1c	

Geophone	Easting (m)	Northing (m)	Elevation (m)	Sensor	Comments
S6-1	395290	6895701	598	1C	Station S6 located in a
S6-2	395271	6895662	565	3C	cracked area (terrace)
S6-3	395263	6895704	590	1C	next to SW ravine
S6-4	395265	6895660	564	1C	
S6-5	395264	6895685	574	1C	10 m from stream
S6-6	395291	6895665	578	1C	
S6-7	395299	6895683	590	1C	Along small crack
S7-1	395580	6895589	465	3C	Station S7 installed in
S7-2	395566	6895557	448	1C	middle of slope and
S7-3	395540	6895575	466	1C	middle of refraction profile
S7-4	395540	6895601	482	1C	Generally exposed to
S7-5	395579	6895625	487	1C	rock falls
S7-6	395609	6895619	474	1C	
S7-7	395609	6895570	447	1C	
S8-1	395374	6895434	394	3C	Station S8 located on a
S8-2	395349	6895432	396	1C	stony (and cracked)
S8-3	395346	6895453	409	1C	terrace above the ravine
S8-4	395375	6895456	412	1C	
S8-5	395403	6895445	400	1C	
S8-6	395401	6895424	387	1C	
S8-7	395374	6895414	384	1C	
S9-1	395743	6895474	373	3C	Station S9 near landing
S9-2	395727	6895506	387	1C	platform P5
S9-3	395751	6895455	365	1C	
S9-4	395781	6895459	363	1C	
S9-5	395723	6895478	378	1C	
S9-6	395713	6895455	369	1C	
S9-7	395747	6895493	379	1C	Close to a big tree
S10-1	395681	6895178	193	3C	Station S10 deployed
S10-2	395664	6895213	217	1C	above a small cliff in lower
S10-3	395693	6895212	212	1C	part of the slide
S10-4	395724	6895176	174	1C	
S10-5	395688	6895155	175	1C	
S10-6	395664	6895146	175	1C	
S10-7	395639	6895173	200	1C	

Appendix B.5: The picked arrival times for the five active shots SP1 to SP2. The first column is the komponent number for all the station as they are numbered in the data. In the second column is the corresponding number of the components as they are labeled when the coordinates were measured in the field. In the second column the 3-component geophone is marked with bold numbers. Such that for example for Station 5m the components 1,2 and three in the data are those which is in the 3-comopnent geophone.

Data	Frery	SP1	SP2	SP3	SP4	SP5
S1	S1					
0	1	11.31.00.096	12.52.00.122	13.48.00.165		
1	2	11.31.00.103	12.52.00.128	13.48.00.173		
2	3	11.31.00.137	12.52.00.123			
3	**4_1**					
4	**4_2**					
5	**4_3**					
6	5	11.31.00.094				
7	6	11.31.00.132	12.52.00.131			
8	7					
S2	S2					
0	1	11.31.00.107	12.52.00.170			09.17.00.312
1	2	11.31.00.078	12.52.00.153			09.17.00.282
2	3	11.31.00.102	12.52.00.157	13.48.00.204		
3	4	11.31.00.064				
4	5	11.31.00.053	12.52.00.147			
5	6			13.48.00.201		
6	**7_1**					
7	**7_2**					
8	**7_3**					
S3	S3					
0	1	11.31.00.090	12.52.00.103	13.48.00.145		
1	2	11.31.00.096	12.52.00.112		08.09.00.184	
2	3	11.31.00.092	12.52.00.115	13.48.00.155	08.09.00.187	
3	**4_1**					
4	**4_2**					
5	**4_3**					
6	5					
7	6					

8	7					
S4	S4					
0	1	11.31.00.137	12.52.00.088			
1	2	11.31.00.114	12.52.00.075	13.48.00.099	08.09.00.130	09.17.00.207
2	3	11.31.00.126	12.52.00.082	13.48.00.109		
3	4	11.31.00.130	12.52.00.087	13.48.00.115		
4	5	11.31.00.101	12.52.00.081	13.48.00.117		09.17.00.223
5	6	11.31.00.136	12.52.00.091			09.17.00.226
6	**7_1**					
7	**7_2**					
8	**7_3**					
S5	S5					
0	1	11.31.00.157	12.52.00.088	13.48.00.083	08.09.00.113	09.17.00.182
1	**2_1**					
2	**2_2**					
3	**2_3**					09.17.00.185
4	3		12.52.00.083	13.48.00.082		
5	4	11.31.00.154		13.48.00.083	08.09.00.113	09.17.00.175
6	5		12.52.00.081	13.48.00.082	08.09.00.114	
7	6		12.52.00.098	13.48.00.097	08.09.00.120	09.17.00.197
8	7			13.48.00.081		
S6	S6					
0	1				08.09.00.136	09.17.00.202
1	**2_1**					
2	**2_2**					
3	**2_3**					
4	3		12.52.00.090	13.48.00.110	08.09.00.129	09.17.00.192
5	4	11.31.00.141	12.52.00.104	13.48.00.119		
6	5	11.31.00.138	12.52.00.097			
7	6	11.31.00.133	12.52.00.102	13.48.00.118		
8	7		12.52.00.100	13.48.00.126	08.09.00.135	
S7	S7					
0	**1_1**					
1	**1_2**					
2	**1_3**					
3	2	11.31.00.150	12.52.00.078	13.48.00.059	08.09.00.095	09.17.00.161
4	3	11.31.00.155	12.52.00.078	13.48.00.067	08.09.00.104	09.17.00.173
5	4	11.31.00.146	12.52.00.072	13.48.00.058	08.09.00.089	09.17.00.161
6	5	11.31.00.155	12.52.00.088	13.48.00.051	08.09.00.093	09.17.00.160

7	6		12.52.00.095	13.48.00.068	08.09.00.103	09.17.00.174
8	7	11.31.00.177	12.52.00.099	13.48.00.082	08.09.00.111	09.17.00.190
S8	S8					
0	**1_1**					
1	**1_2**					
2	**1_3**					
3	2					
4	3	11.31.00.177	12.52.00.112	13.48.00.084		
5	4	11.31.00.184	12.52.00.121	13.48.00.088		
6	5	11.31.00.192	12.52.00.117	13.48.00.084		
7	6	11.31.00.165	12.52.00.111	13.48.00.086		
8	7	11.31.00.182	12.52.00.111	13.48.00.086		
S9	S9					
0	**1_1**					
1	**1_2**					
2	**1_3**					
3	2		12.52.00.127		08.09.00.071	
4	3	11.31.00.193	12.52.00.120	13.48.00.076	08.09.00.055	
5	4	11.31.00.195	12.52.00.123	13.48.00.078	08.09.00.066	
6	5	11.31.00.204	12.52.00.131	13.48.00.083	08.09.00.063	09.17.00.133
7	6			13.48.00.086	08.09.00.067	
8	7			13.48.00.088	08.09.00.062	
S10	S10					
0	**1_1**					
1	**1_2**					
2	**1_3**					
3	2				08.09.00.067	09.17.00.061
4	3	11.31.00.256	12.52.00.180	13.48.00.076	08.09.00.071	
5	4		12.52.00.171	13.48.00.079	08.09.00.069	
6	5	11.31.00.217	12.52.00.167	13.48.00.083	08.09.00.066	09.17.00.045
7	6	11.31.00.234			08.09.00.067	09.17.00.045
8	7	11.31.00.254	12.52.00.183	13.48.00.086		09.17.00.052

APPENDICS C: Picking arrivaltimes

Event nr. 2. Example of the picking process on the waveforms from all the components at station S6. I have not picked first arrival on the first component because it was difficult the see the onset clear enough.

seconds (in the figure: 451.1sec to 452.8sec)